Studies of Phosphoproteomic Changes Induced by Nucleophosmin-Anaplastic Lymphoma Kinase (ALK) Highlight Deregulation of Tumor Necrosis Factor (TNF)/Fas/TNF-related Apoptosis-induced Ligand Signaling Pathway in ALK-positive Anaplastic Large Cell Lymphoma*[S]

Fang Wu‡, Peng Wang§, Jingdong Zhang¶, Leah C. Young§, Raymond Lai§‖, and Liang Li‡‖****

The oncogenic fusion protein nucleophosmin-anaplastic lymphoma kinase (NPM-ALK), found exclusively in a subset of ALK-positive anaplastic large cell lymphoma, promotes tumorigenesis by exerting its constitutively active tyrosine kinase activity. Thus, characterization of the NPM-ALK-induced changes in the phosphoproteome will likely provide insights into the biology of this oncoprotein. To achieve this goal, we used a strategy of combining sequential affinity purification of phosphopeptides and LC/MS. GP293 cells transfected with either *NPM-ALK* or an *NPM-ALK* mutant with decreased tyrosine kinase activity (negative control) were used. We identified 506 phosphoproteins detectable in NPM-ALK-expressing cells but not in the negative control. Bioinformatics analysis revealed that these phosphoproteins carry a wide diversity of biological functions, some of which have not been described in association with NPM-ALK, such as the tumor necrosis factor (TNF)/Fas/tumor necrosis factor-related apoptosis-induced ligand (TRAIL) signaling pathway and the ubiquitin proteasome degradation pathway. In particular, modulations of the TNF/Fas/TRAIL pathway by NPM-ALK were supported by our antibody microarray data. Further validation of the TNF/Fas/TRAIL pathway was performed in ALK$^+$ anaplastic large cell lymphoma (ALCL) cell lines with knockdown of NPM-ALK using short interference RNA, resulting in the loss of the tyrosine phosphorylation of tumor necrosis factor receptor-associated protein 1 (TRAP1) and receptor-interacting protein 1, two crucial TNF signaling molecules. Functional analyses revealed that knockdown of TRAP1 facilitated cell death induced by TRAIL or doxorubicin in ALK$^+$ ALCL cells. This suggests that down-regulation of TRAP1 in combination with TRAIL or doxorubicin might be a potential novel therapeutic strategy for ALK$^+$ ALCL. These findings demonstrated that our strategy allowed the identification of novel proteins downstream of NPM-ALK that contribute to the maintenance of neoplastic phenotype and holds great potential for future studies of cellular tyrosine kinases in normal states and diseases. *Molecular & Cellular Proteomics 9:1616–1632, 2010.*

Anaplastic lymphoma kinase (ALK)[1]-positive anaplastic large cell lymphoma (ALK$^+$ ALCL) is a subtype of T/null cell non-Hodgkin lymphoma that is characterized by its consistent expression of CD30 and anaplastic cytology (1). ALK$^+$ ALCL is relatively uncommon among adults, accounting for ~3% of adult non-Hodgkin lymphoma, whereas it is frequent in children, representing 10–20% of all lymphoma (2). Approximately 80% of ALK$^+$ ALCL tumors carry the *t*(2;5)(p23;q35) chromosomal translocation that fuses the tyrosine kinase do-

From the ‡Department of Chemistry, University of Alberta, Edmonton, Alberta T6G 2G2, Canada, §Department of Laboratory Medicine and Pathology, University of Alberta and Cross Cancer Institute, Edmonton, Alberta T6G 1Z2, Canada, and ¶Department of Surgery, University of Alberta, Edmonton, Alberta T6G 2B7, Canada

Received, April 2, 2010

Published, MCP Papers in Press, DOI 10.1074/mcp.M000153-MCP201

[1] The abbreviations used are: ALK, anaplastic lymphoma kinase; ALK$^+$ ALCL, ALK-positive anaplastic large cell lymphoma; NPM, nucleophosmin; SCX, strong cation exchange; PI3K, phosphatidylinositol-4,5-bisphosphate 3-kinase; STAT, signal transducer and activator of transcription; ERK, extracellular signal-regulated kinase; mTOR, mammalian target of rapamycin; MAPK, mitogen-activated protein kinase; TNF, tumor necrosis factor; DAPK3, death-associated protein kinase 3; CRADD, CASP2 and RIPK1 domain-containing adaptor with death domain; AKT, RAC-α serine/threonine-protein kinase; TRAIL, tumor necrosis factor-related apoptosis-induced ligand; TRAP1, tumor necrosis factor receptor-associated protein 1; RIP, receptor-interacting protein 1; JAK, Janus kinase; NIPA, nuclear interacting partner of ALK; JNK, c-Jun N-terminal kinase; FAF1, Fas-associated factor 1; NRF, NF-κB-repressing factor; GAK, cyclin G-associated kinase; HB, Histidine-Biotin; SHC, Src homology 2 domain-containing-transforming protein C1; RFFL:E3 ubiquitin-protein ligase rififylin; TOPRS:E3 ubiquitin-protein ligase Topors; PTB, Polypyrimidine tract-binding protein; ATIC, 5-aminoimidazole-4-carboxamide ribonucleotide formyltransferase.

main of ALK with the oligomerization domain of the nucleophosmin (NPM) protein. This chromosomal translocation results in the formation of the chimeric protein NPM-ALK (3–7). NPM-ALK has been shown to have propensity to dimerize, and this process triggers autophosphorylation of NPM-ALK and results in constitutive activation of the ALK tyrosine kinase. Once activated, NPM-ALK binds, phosphorylates, and constitutively activates a host of proteins involved in various cellular signaling pathways, including those of PI3K/RAC-α serine/threonine-protein kinase (AKT) (8, 9), JAK/STAT (10), mTOR (11–13), mitogen-activated protein kinase/extracellular signal-regulated kinase kinase (MEK)/ERK (14), and Ras/MAPK (15).

As a tyrosine kinase, major attention was drawn to NPM-ALK in identifying the tyrosine phosphorylation, whereas other aspects of this oncogenic protein were not fully explored. Two LC/MS studies were performed previously (16, 17). Using quantitative LC/MS, Boccalatte *et al.* (16) reported 47 phosphoproteins in a panel of ALK^+ ALCL cell lines that showed significant changes in their phosphorylation status upon ALK inhibition by short hairpin RNA or a tyrosine kinase inhibitor. Using LC/MS, Rush *et al.* (17) recently found ~70 phosphoproteins from each of the two ALK^+ ALCL cell lines, although whether the phosphorylation of these proteins is related to NPM-ALK was not determined. In both studies, only phosphotyrosine-containing proteins were captured by using a phosphotyrosine antibody immobilized to a solid phase prior to LC/MS analysis.

However, mounting evidence has shown that NPM-ALK-induced signaling can culminate in the activation of oncogenic pathways via regulating serine/threonine phosphorylation (*e.g.* mTOR, c-Jun, nuclear interacting partner of ALK (NIPA), and AKT) (13, 18, 19). It is highly possible that NPM-ALK induces serine/threonine phosphorylation of downstream targets through recruitment and activation of various serine/threonine kinases like previously reported JNK and ERK (12, 18). In this regard, we have reported that NPM-ALK physically interacts with multiple serine/threonine kinases, including ribosomal protein S6 kinase α-3, serine/threonine/tyrosine kinase 1 (STYK1), serine/threonine-protein kinase PRP4, and serine/threonine-protein kinase PCTAIRE-3 (20). Therefore, comprehensive characterization of phosphoproteomic changes (*i.e.* serine, threonine, and tyrosine phosphorylation) induced by NPM-ALK will likely further our understanding of the pathobiology of NPM-ALK.

Although comprehensive characterization of phosphoproteomic changes induced by oncogenic tyrosine kinases (such as NPM-ALK) is highly useful, this approach is met with multiple technical challenges. It is intrinsically difficult to detect phosphoproteins because the phosphopeptides produced from the phosphoproteins are generally present at a much lower amount compared with their native counterparts. In an attempt to overcome this difficulty, several enrichment approaches that are designed to isolate phosphorylated amino acid residues have been described, and they include IMAC through metal complexation with the phosphate group (21–23), acid-based interaction with titanium oxide (24–28), and solution charge-based enrichment by strong cation exchange chromatography (23, 29). Specific capture of phosphopeptides is possible by elimination of the phosphate group and subsequent introduction of an affinity tag (30) or conversion to methyl ester derivatives (21, 31, 32). In addition, several groups have combined various ion exchange approaches with IMAC to further enrich phosphopeptides prior to LC/MS/MS analysis (33–35). These works and others reported were mainly focused on improving the enrichment of phosphopeptides to facilitate the detection of as many phosphopeptides as possible. However, because tyrosine residues are present at much lower concentrations than serine or threonine (*i.e.* serine/threonine/tyrosine ratio is 1800:200:1), important proteins carrying phosphotyrosine residues often escape detection and are under-represented in the final results. To address this issue, several research groups recently reported the utilization of anti-phosphotyrosine antibodies to specifically enrich the phosphotyrosine-containing peptides within the digest (16, 17, 36) or intact protein prior to digestion (32). The use of anti-phosphotyrosine antibody alone, as used in the two previous studies of NPM-ALK (16, 17), is prone to nonspecific proteins binding to the anti-phosphotyrosine antibodies, resulting in a high background that may prevent the detection of the relatively weak signals of phosphotyrosine-containing peptides. Specific capture of phosphotyrosine-containing peptides has been enhanced by phosphotyrosine protein enrichment followed by IMAC (37, 38). Recently, Heck and co-workers (39) have reported an optimized enrichment method for phosphotyrosine peptides based on immunoaffinity purification. This method allowed a high level of enrichment; they were able to identify 1112 unique phosphotyrosine peptides derived from 4 mg of starting materials. However, biologically important proteins carrying phosphoserine and phosphothreonine residues were excluded with this approach. To identify both phosphotyrosine-containing proteins and phosphoserine-/phosphothreonine-containing proteins, parallel experiments involving in IMAC enrichment mainly for phosphoserine/phosphothreonine protein identification and anti-phosphotyrosine enrichment mainly for phosphotyrosine protein identification have been reported (23). However, this work required a doubled amount of the starting materials.

To characterize the phosphoproteomic changes induced by NPM-ALK in a comprehensive and efficient manner, we developed a strategy and applied it to enrich phosphopeptides prior to the LC/MS analysis. The design of this enrichment strategy is based on three theoretical advantages. 1) It enables comprehensive identification of all three types of phosphorylated peptides. 2) It facilitates the detection of the phosphotyrosine-containing peptides despite their relatively low abundance compared with phosphoserine- and phosphothreonine-containing peptides. 3) It does not require parallel

experiments; *i.e.* the same starting materials were used for profiling both phosphoserine-/phosphothreonine-containing proteins and phosphotyrosine-containing proteins. In the first step, all the phosphopeptides were enriched by using IMAC. In the second step, using an anti-phosphotyrosine specific antibody, we separated the phosphotyrosine pool from that of phosphoserine and phosphothreonine. Because of the prior enrichment by IMAC, the nonspecific protein binding to the phosphotyrosine antibody will be minimized. The phosphoserine/phosphothreonine pool was fractionated by strong cation exchange chromatography to facilitate their detection by LC/MS. Our results suggest that this strategy is highly useful in the comprehensive characterization of the phosphoproteome, particularly in enhancing our ability to detect phosphotyrosine peptides.

One of the key objectives of this study was to comprehensively assess the phosphoproteomic changes induced by oncogenic kinase NPM-ALK that can serve as a proof of principle for future related biological studies. To achieve this goal, our experimental approach was designed to compare the qualitative phosphoproteomic changes between unaltered *NPM-ALK*- and *NPM-ALK^{FFF}* mutant-transfected cells, focusing on similar absolute changes in phosphorylation statuses, by using our strategy. We did not use a quantitative proteomics approach to analyze the phosphoproteomic changes induced by NPM-ALK because of the special property of this oncoprotein. Most of the previous reports (40–42) and our previous publication (43) have shown that phosphorylation of proteins downstream of NPM-ALK were only present in the presence of NPM-ALK; in the absence of NPM-ALK, the phosphorylation statuses of proteins downstream of NPM-ALK were lost. Using quantitative proteomics approaches, such as stable isotope labeling with amino acid in cell culture or isobaric tags for relative and absolute quantitation, will sacrifice the sensitivity of identification. Therefore, in this study, we used a qualitative phosphoproteomics approach instead of using a quantitative phosphoproteomics approach.

In this study, we applied this protocol to compare the phosphorylation profile changes between the unaltered *NPM-ALK*- and *NPM-ALK^{FFF}* mutant-transfected cells and identify a set of phosphorylated proteins likely associated with NPM-ALK activity. It was found that the phosphoproteins identified regulate a diversity of key cellular pathways, some of which have never been reported to be associated with NPM-ALK. To document the biological relevance of these identified phosphoproteins, validation experiments were performed using *NPM-ALK*- and *NPM-ALK^{FFF}* mutant-transfected cells as well as ALK$^+$ ALCL cells. The TNF/Fas/tumor necrosis factor-related apoptosis-induced ligand (TRAIL) signaling pathway was validated to be modulated by NPM-ALK in ALK$^+$ ALCL. Functional analysis showed that knockdown of tumor necrosis factor receptor-associated protein 1 (TRAP1), one of the crucial TNF/Fas/TRAIL signaling molecules, enhanced TRAIL- or chemotherapeutic drug doxorubicin-induced cell death. These findings provide a potential therapeutic strategy for ALK$^+$ ALCL and novel insight into the NPM-ALK-mediated lymphomagenesis.

EXPERIMENTAL PROCEDURES

Gene Construction and Mutagenesis—Full-length human *NPM-ALK* cDNA was amplified from a pcDNA-*NPM-ALK* plasmid, a kind gift from Dr. S. Morris (St. Jude's Children Research Hospital, Memphis, TN) and inserted into the HB vector as described previously (20). The *NPM-ALK^{FFF}* mutant was generated by mutating Tyr^{338}, Tyr^{342}, and Tyr^{343} to phenylalanine using the QuikChangeXL site-directed mutagenesis kit (Stratagene, La Jolla, CA) as described previously (43). The sequences of *NPM-ALK* and *NPM-ALK^{FFF}* were subsequently confirmed by DNA sequence analysis.

Cell Culture and Gene Transfection—GP293 (a modified version of the HEK 293 human embryonic kidney cell line; Clontech) was cultured in Dulbecco's modified Eagle's medium (Sigma) supplemented with 10% heat-inactivated fetal bovine serum and 1% penicillin. GP293 cells were transiently transfected with HB-tagged *NPM-ALK* or HB-tagged *NPM-ALK^{FFF}* mutant using Lipofectamine™ 2000 transfection reagent (Invitrogen) as described previously (20). Cell lysates were collected for further mass spectrometric analysis after 24-h transfection.

Two ALK$^+$ ALCL cell lines (Karpas 299 and SU-DH-L1), both of which have been described previously (44), were maintained in RPMI 1640 medium (Invitrogen) supplemented with 10% fetal bovine serum. All the cells were cultured under an atmosphere of 95% O_2 and 5% CO_2 in 98% humidity at 37 °C.

Cell Lysate and In-solution Digestion—Fig. 1 shows the work flow used to profile the phosphoproteome of *NPM-ALK*-transfected cells (*i.e. NPM-ALK*-transfected cells and *NPM-ALK^{FFF}* mutant-transfected cells). Cells were lysed in CelLytic™ M buffer (Sigma), 1 mM phenylmethylsulfonyl fluoride, protease inhibitor mixture, and phosphatase inhibitor mixture (Sigma). The lysates were precleared at 20,000 × *g* for 15 min. A bicinchoninic acid (BCA) assay kit (Bio-Rad) was used to determine the protein concentration of the resulting lysate. About 20 mg of each sample were used for further analysis. To remove the salts and other impurities, acetone was added into cell lysates with vortexing to a final acetone concentration of 80%. The mixture was incubated at −80 °C for 10 min and then stored at −20 °C overnight. The mixture was then centrifuged at 20,000 × *g* for 10 min. After decanting the supernatant, the pellets were dissolved with 1% (w/v) RapiGest (Waters) with intermittent vortexing. The protein mixture was reduced with 10 mM DTT for 1 h at 37 °C and then alkylated with 55 mM iodoacetamide for 1 h at room temperature. Trypsin solution was added into the protein solution at a ratio of 1:50 after 10-fold dilution, and the mixture was incubated at 37 °C overnight. 10% TFA was added to the peptide mixture to make the final TFA concentration ~0.5% (pH < 2). The mixture was incubated at 37 °C for 45 min and then centrifuged at 20,000 × *g* for 10 min, and the supernatant was transferred into a fresh vial for further sample workup.

IMAC—Prior to IMAC, peptides were desalted by using an Agilent 1100 HPLC system using a 4.6 × 50-mm C_{18} column (Varian, Ontario, Canada) and then lyophilized. Phosphopeptide enrichment by IMAC was performed as described previously (21) except that peptides were not converted to methyl ester derivatives. After resolubilization with 30% ACN mixed with 250 mM acetic acid, the peptides were loaded onto pre-equilibrated iron IMAC resin (Phos-Select iron affinity gel, Sigma). The resin was washed three times with 30% ACN and 250 mM acetic acid and two times with water after overnight incubation at 4 °C. The phosphopeptides were then released from the resin with 400 mM ammonium hydroxide.

Tyr(P)-based Immunoaffinity Purification—After IMAC elution, the proportion of phosphotyrosine-containing peptides was further enriched using the PhosphoScan kit (Tyr(P)^{100}) (Cell Signaling Technol-

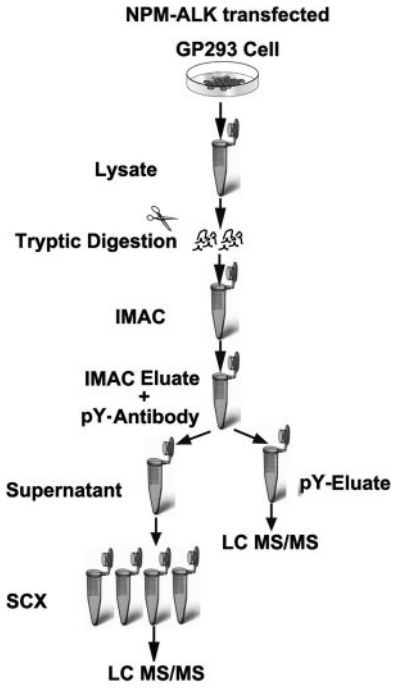

FIG. 1. **Work flow for analysis of NPM-ALK-induced phosphoproteins.** *NPM-ALK*-transfected GP293 cells were lysed and digested with trypsin. The phosphopeptides, including phosphotyrosine, phosphoserine, and phosphothreonine peptides, were first enriched by IMAC. The phosphotyrosine-containing peptides were further enriched by using anti-phosphotyrosine (*pY*) antibody followed by tandem mass spectrometry analysis. The flow-through containing phosphoserine and phosphotyrosine peptides was fractionated by strong cation exchange, and then individual fractions were analyzed by reverse phase liquid chromatography and tandem mass spectrometry The *NPM-ALK*^{FFF}-transfected cells, used as a negative control, were treated in the same manner.

ogy, Inc., Danvers, MA) according to the manufacturer's instructions. Briefly, the phosphopeptides were lyophilized and then redissolved in immunoaffinity purification buffer (50 mM MOPS at pH 7.2, 10 mM sodium phosphate, and 50 mM NaCl). The peptide mixture was then incubated with immobilized anti-phosphotyrosine antibody beads at 4 °C overnight. The antibody beads were collected at 1500 × *g* for 5 min, and the supernatant containing phosphoserine and phosphothreonine peptides was retained and stored at −20 °C for further processing. The beads were washed twice with 100 μl of immunoaffinity purification buffer and twice with rinse buffer (100 mM Tris and 100 mM NaCl). The phosphotyrosine-containing peptides were eluted from the beads by using 0.1% TFA, desalted, quantified by UV absorbance (45), and then subjected to reverse phase LC/MS/MS analysis.

Strong Cation Exchange (SCX) Liquid Chromatography and Mass Spectrometric Analysis—A 2.1 × 250-mm polySULFOETHYL™ A column (5-μm diameter, 300-Å pore) (PolyLC, Columbia, MD) was used for the SCX separation of the phosphoserine- and phosphothreonine-containing peptide mixture. Solvent A (5 mM KH_2PO_4, pH 2.7) and solvent B (solvent A with 500 mM KCl) were used to develop a salt gradient (0–7% for 5 min, 7–42% for 35 min, and 42–100% for 2 min). All the samples collected from SCX were desalted on an Agilent 1100 HPLC system and quantified by UV absorbance. Tandem mass spectrometry analysis was performed as described previously (20, 46). Approximately 1.0 μg of peptides from individual fraction was analyzed using a Q-TOF Premier mass spectrometer (Waters) equipped with a nanoACQUITY Ultra Performance LC system (Waters). Peptide solution from each SCX fraction was injected onto a 75-μm × 100-mm Atlantis dC_{18} column (Waters). Solvent A consisted of 0.1% formic acid in water, and solvent B consisted of 0.1% formic acid in ACN. Peptides were separated using a 120-min gradient (6–25% solvent B for 95 min, 30–50% solvent B for 10 min, 50–90% solvent B for 10 min, and 90–5% solvent B for 5 min) and electrosprayed into the mass spectrometer fitted with a nanoLockSpray source at a flow rate of 300 nl/min. Mass spectra were acquired from *m/z* 300 to 1600 for 0.8 s followed by four data-dependent MS/MS scans from *m/z* 50 to 1900 for 1.0 s each. The collision energy used to perform MS/MS was automatically varied according to the mass and charge state of the eluting peptide. A mass calibrant (*i.e.* lock mass) was infused at a rate of 250 nl/min, and an MS scan was acquired for 1 s every 1 min throughout the run. A precursor ion exclusion strategy was applied to exclude relatively high abundance peptides identified from the adjacent two SCX fractions to enable additional less abundant peptides to be analyzed and identified. An exclusion list was generated as described previously (46).

Database Search and Data Analysis—Raw MS/MS data were lock mass-corrected, deisotoped, and converted to peak list files by ProteinLynx Global Server 2.2.5 (Waters). Protein identification was performed by using the Mascot 2.2 search engine (Matrix Science) for searching the Swiss-Prot database (version 57.4, 410,518 sequences). Searching was restricted *Homo sapiens* (20,401 sequences) and performed using the following parameters: fixed modification, carbamidomethyl (Cys); variable modifications, oxidation (Met) and phosphorylation on serine, threonine, or tyrosine; enzyme, trypsin; missed cleavages, 1; peptide tolerance, 30 ppm; MS/MS tolerance, 0.2 Da; peptide charge, 1+, 2+, and 3+. Peptide information was extracted to an Excel data sheet from the search results using a in-house written program. All the peptides that had scores lower than the Mascot identification threshold were removed as well as redundant peptides and proteins. All the identified peptides were above the Mascot threshold score for identity with a confidence level of >95%. The false positive rate was determined by using the target-decoy search strategy (47). The overall false positive rate was <1%. The data set of *NPM-ALK*-transfected GP293 cells was filtered against a control data set of *NPM-ALK*^{FFF} mutant-transfected GP293 cells using an in-house developed program. An increased molecular mass of 79.96 Da on a tyrosine, serine, or threonine residue was indicative of phosphorylation. The spectra and phosphorylation site assignment of all NPM-ALK-induced proteins were checked manually based on the following rules. First of all, for serine and threonine phosphorylation site localization, we searched H_3PO_4 neutral losses from fragment ions (b ions and/or y ions). A −18 Da modification corresponding to the mass difference between serine and dehydroalanine or threonine and 2-aminodehydrobutryic acid was also considered. Second, because phosphotyrosine residues do not normally undergo neutral loss, the cognate pair of the fragment ion (b_i, b_i − 79.96 and/or y_i, y_i − 79.96) or fragment ions (b and/or y ion) containing a phosphate group were expected to be found in the spectrum. Additionally, immonium ion at *m/z* 216 was also investigated in the phosphotyrosine-containing peptides. Third, unambiguous localization of a phosphorylation site could further be obtained by a continuous fragment ion series around the phosphorylated residue. Ambiguous phosphorylation site identification was excluded from the list. A summary of Mascot search results, peptide identifications, and phosphorylation site assignments is shown in the supplemental materials.

Antibody Array Studies—XP725 Panorama Antibody Microarray (Sigma) contains 725 different antibodies spotted in duplicate on nitrocellulose-coated glass slides. These antibodies represent families of proteins known to be involved in a variety of different biological

pathways. The antibody array experiment was performed on *NPM-ALK*- and *NPM-ALK^{FFF}* mutant-transfected GP293 cells according to the manufacturer's instructions. *NPM-ALK* and *NPM-ALK^{FFF}* mutant were transfected into GP293 cells. The cells were grown to 80% confluence and washed twice with ice-cold PBS. Cell lysates were collected. The protein concentration was determined by the Bradford protein assay (Sigma). The samples were diluted to 1 mg/ml. About 150 μg of extract was used for labeling. The *NPM-ALK*-transfected sample was labeled with Cy5, and the *NPM-ALK^{FFF}*-transfected sample was labeled with Cy3. The non-conjugated free dye was removed from the labeled sample by using SigmaSpin Post-Reaction Clean-Up columns (Sigma) and centrifugation at 750 $\times$ *g* at 4 °C. Labeling efficiency was verified by the dye to protein molar ratio based on the manufacturer's instructions. Then, the Cy5-labeled NPM-ALK sample was mixed with the Cy3-labeled NPM-ALK^{FFF} mutant sample in a 1:1 molar ratio. The labeled protein mixture was then incubated with the antibody microarray at room temperature on a rocking shaker for 30 min. The array slide was washed with TBS-Tween 20 (20 mM Tris-HCl, pH 7.5, 137 mM NaCl, and 0.1% Tween 20) twice for 5 min and immersed in water for 2 min. Once dry, the array was scanned on Genepix 4000B (Molecular Devices, Sunnyvale, CA) with a 532 and 635 nm laser. Fluorescence intensity measurements from the array element were compared with the local background, and then background subtraction was performed. Before normalization, spots showing defects were manually flagged. Spots with intensities for both channels (sum of the medians) lower than the sum of the mean backgrounds were also discarded. Fluorescence intensities were normalized by reference proteins. Inconsistent duplicates were excluded. The ratios of the duplicated spots were averaged. The cutoff level used to determine significant changes was chosen to be a $\geq$2-fold change in expression between samples. This cutoff level has become the standard in expression microarray analysis and has also been used previously in antibody array experiments (48, 49). The statistical Z test was used to obtain the *p* value ($p < 0.003$).

Bioinformatics Analysis—Functional pathway and network analysis was generated through the use of Ingenuity Pathway Analysis software (Ingenuity Systems, Redwood, CA). The significance of the association between the data set and the canonical pathway was measured in two ways. 1) The ratio of the number of proteins that map to the canonical pathway was calculated, and 2) Fisher's exact test was used to calculate a *p* value determining the probability of the association between the protein in the data set and the canonical pathway.

Western Blotting and Immunoprecipitation—Western blot and immunoprecipitation were performed using standard techniques as described previously (10, 50, 51). Briefly, 2 mg of cell lysates was incubated with an antibody overnight at 4 °C. Protein A/G PLUS-agarose (EMD Chemical, Inc., Gibbstown, NJ) was added and incubated with gentle rotation at 4 °C overnight. The immunocomplex was washed with cold PBS three times followed by washing with radioimmune precipitation assay buffer (25 mM Tris-HCl, pH 7.6, 150 mM NaCl, 1 mM Na_2EDTA, I mM EGTA,1% Nonidet P-40, 1% sodium deoxycholate, 2.5 mM sodium pyrophosphate, 1 mM β-glycerophosphate, 1 mM Na_3VO_4, 1 μg/ml leupeptin, and 0.1% SDS). The complex was subjected to SDS-PAGE and transferred onto nitrocellulose membranes. After blotting for 1 h at room temperature, the membranes were incubated overnight at 4 °C in primary antibody, washed three times in TBS-Tween 20, incubated for 1 h at room temperature with a secondary antibody, and finally washed three times with TBS-Tween 20. Blots were visualized using enzyme chemiluminescence (ECL, Amersham Biosciences). The following antibodies were used for immunoprecipitation and immunoblotting: anti-phosphotyrosine antibody (Cell Signaling Technology, Inc., Ontario, Canada), anti-receptor-interacting protein 1 (RIP) antibody (Cell Signaling Technology, Inc., Ontario, Canada), mouse monoclonal anti-TRAP1 antibody (Abcam, Cambridge, MA), anti-phospho-STAT3 antibody (Cell Signaling Technology, Inc., Ontario, Canada), anti-STAT3 antibody (BD Biosciences), anti-phospho-SHC antibody (Cell Signaling Technology, Inc., Ontario, Canada), anti-SHC antibody (Cell Signaling Technology, Inc., Ontario, Canada), anti-Fas-associated factor 1 (FAF1) antibody (Abcam), anti-ALK antibody (Cell Signaling Technology, Inc., Ontario, Canada), anti-phospho-ERK1/2 antibody (Cell Signaling Technology, Inc., Ontario, Canada), anti-ERK1/2 antibody (Cell Signaling Technology, Inc., Ontario, Canada), anti-phospho-Src (Tyr^{418}) antibody (Cell Signaling Technology, Inc., Ontario, Canada), and anti-phospho-Src (Tyr^{527}) antibody (Cell Signaling Technology, Inc., Ontario, Canada).

Short Interference RNA (siRNA)—For each experiment, SU-DH-L1 cells (7.5 $\times$ 10^6 cells) were transfected with siRNA for NPM-ALK (L-003103, Thermo Scientific) or siRNA for TRAP1 (L-010104, Thermo Scientific) using scrambled non-targeting siRNA (D-001810, Thermo Scientific) as the negative control. In both cases, a BTX 830 electroporation transfection instrument (Harvard Apparatus, Inc.) was used. Transfected cells were cultured for 48 h for further cell viability or Western blot analysis.

Cell Viability Assay—SU-DH-L1 cells transfected with either TRAP1 siRNA or scrambled siRNA (10,000 cells) were seeded in each well of a 96-well plate and treated with TRAIL (Alexis Biochemicals, San Diego, CA) or doxorubicin (Calbiochem) for 24 h. A tetrazolium compound (3-(4,5-dimethylthiazol-2-yl)-5-(3-carboxymethoxyphenyl)-2-(4-sulfophenyl)-2*H*-tetrazolioum) was then added to each well, and the number of viable cells was quantified using the Celltiter 96 Aqueous cell proliferation assay (Promega, Madison, WI) and a spectrophotometer (BioTek Instruments Inc., Winooski, VT) according to the manufacturer's protocol (52). Student's *t* test was used to calculate the *p* value. All the experiments were performed triplicate.

RESULTS

Functional Expression of NPM-ALK and NPM-ALK^{FFF} Mutant—The *NPM-ALK* construct was inserted into the HB-tagged vector as described previously (20). The *NPM-ALK^{FFF}* mutant was generated by simultaneous mutation of all three tyrosine residues (Tyr^{338}/Tyr^{342}/Tyr^{343}) present in the ALK kinase activation loop as described previously (43) and illustrated in Fig. 2. We previously found that NPM-ALK^{FFF} has a complete loss of autophosphorylation (detectable by mass spectrometry) and tumorigenicity (assessed by soft agar clonogenic assay) (43), and this mutant was used as a negative control in this study.

After the DNA sequences of *NPM-ALK* and *NPM-ALK^{FFF}* were confirmed, we then determined the expression level and the oncogenic potential of the NPM-ALK proteins expressed. First, we compared the protein levels of NPM-ALK in GP293 cells expressing either *NPM-ALK* or *NPM-ALK^{FFF}* with those in ALK$^+$ ALCL cells. As shown in Fig. 3, the expression levels of NPM-ALK in the transfected GP293 cells were similar to those seen in ALK$^+$ ALCL cells (*i.e.* Karpas 299 and SU-DH-L1 cells). Due to the addition of the HB tag in the two constructed vectors, HB-tagged NPM-ALK and NPM-ALK^{FFF} migrated slightly slower that the NPM-ALK protein expressed in the two ALK$^+$ ALCL cell lines. Second, we further assessed the oncogenic potential of the NPM-ALK proteins by measuring their ability to activate and phosphorylate a panel of

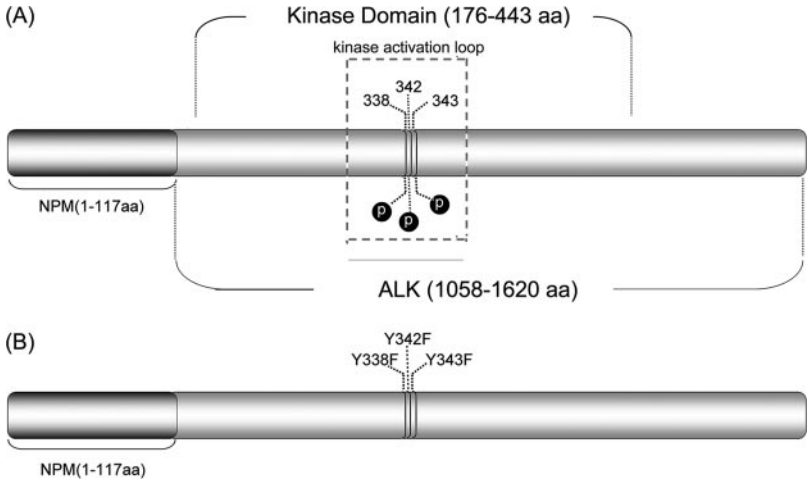

FIG. 2. **Schematic representation of NPM-ALK.** *A*, *NPM-ALK*, showing the location of the kinase domain and the Y*XXX*YY motif within the activation loop. *B*, *NPM-ALK^{FFF}* mutant, which was generated by mutating the three tyrosine residues (Tyr^{338}/Tyr^{342}/Tyr^{343}) within the tyrosine kinase signature domain (Y*XXX*YY) of the activation loop to phenylalanine. *aa*, amino acids.

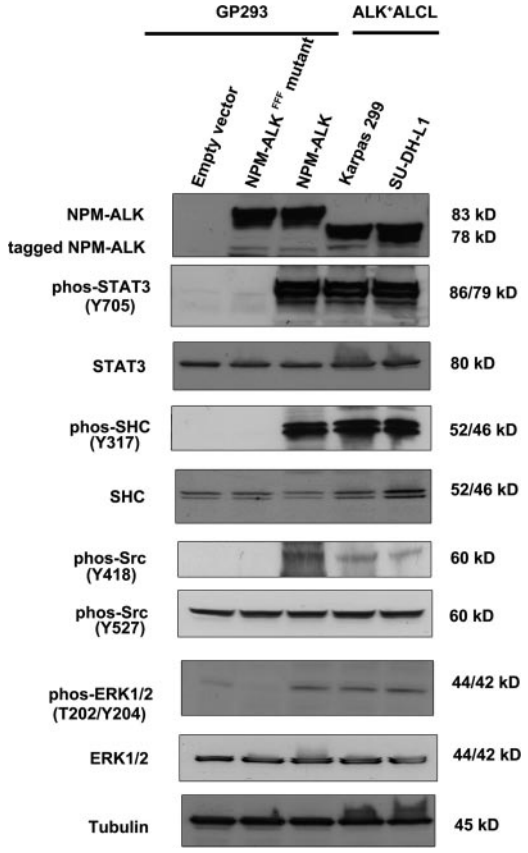

FIG. 3. **Comparison of either *NPM-ALK* or *NPM-ALK^{FFF}* mutant-transfected GP293 cells with ALK$^+$ ALCL cells (Karpas 299 and SU-DH-L1).** Western blot analysis showed the similar expression levels of NPM-ALK in the transfected GP293 cells and in Karpas 299 and SU-DH-L1. STAT3, SHC, Src, and ERK1/2 were phosphorylated (*phos*) in *NPM-ALK*-transfected GP293 cells and ALK$^+$ ALCL cells but not in *NPM-ALK^{FFF}* mutant-transfected GP293. The loading control was tubulin.

downstream effector proteins, including STAT3, SHC, Src, and ERK1/2, all of which are known to be phosphorylated by NPM-ALK (14, 15, 41). As shown in Fig. 3, STAT3, SHC, Src, and ERK1/2 were found to be phosphorylated in cells transfected with *NPM-ALK* but not those transfected with *NPM-ALK^{FFF}*.

Characterization of NPM-ALK-induced Phosphoproteomic Changes—Using the phosphopeptide enrichment protocol illustrated in Fig. 1, in *NPM-ALK*-transfected cells, 4265 phosphopeptides and 5340 phosphorylation sites were found from which a total of 1758 phosphoproteins were identified. In cells transfected with the *NPM-ALK^{FFF}* mutant (negative control), 4798 phosphorylation sites and 3645 phosphopeptides were found from which a total of 1548 phosphoproteins were identified. By subtracting those found in the negative control, there were 506 phosphoproteins (617 phosphopeptides and 767 phosphorylation sites) that were found exclusively in NPM-ALK-expressing cells. Further analysis of this list of phosphopeptides revealed 179 phosphotyrosine peptides (with 180 phosphotyrosine sites) and 323 phosphoserine/threonine peptides (507 phosphoserine sites and 80 phosphothreonine sites). Of the 179 phosphopeptides containing phosphotyrosine, only five also carry phosphoserine and/or phosphothreonine sites. Of the 506 phosphoproteins, only 13 carry both tyrosine and serine/threonine phosphorylation sites. The entire list of phosphopeptides as well as the 506 phosphoproteins is given in supplemental Table S1.

We note that in our experience with proteome analysis of cell extracts the sample-to-sample reproducibility with the precursor ion exclusion strategy (49) is usually over 85%. Thus, the major difference observed in phosphopeptides identified from the two comparative samples should largely reflect the biological difference of the samples. We did not carry out the quantitative or replicate profiling work as the workload would be very high. In addition, the purpose of the profiling work was to generate leads for downstream biological work. Thus, our efforts were focused on carrying out biological functional studies based on the leads generated from the phosphoproteomic profiles and bioinformatics analysis results (see below). However, we would like to make some cautious remarks on the list of phosphopeptides and

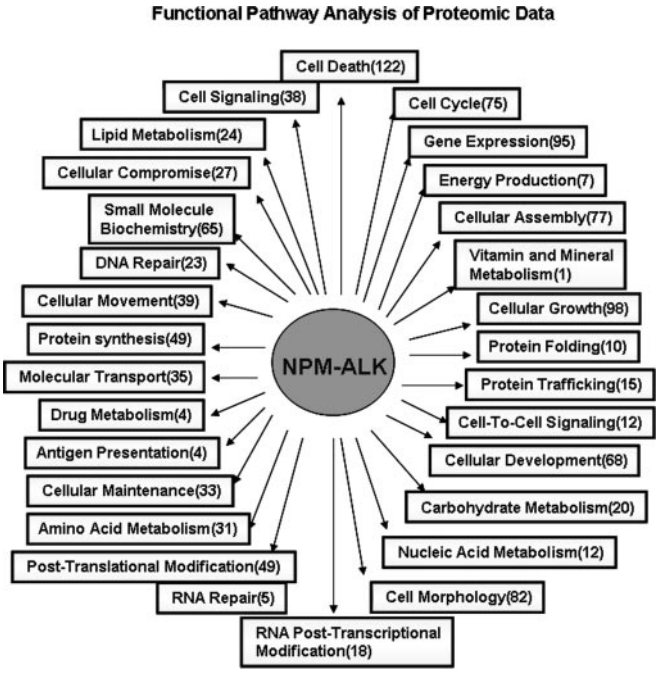

FIG. 4. **Functional pathway analysis of the NPM-ALK-induced phosphoproteins.** The Ingenuity Pathway Analysis software was used to analyze the functional pathways of the NPM-ALK-induced phosphoproteins. The numbers in parentheses represent the number of proteins belonging to the corresponding pathways.

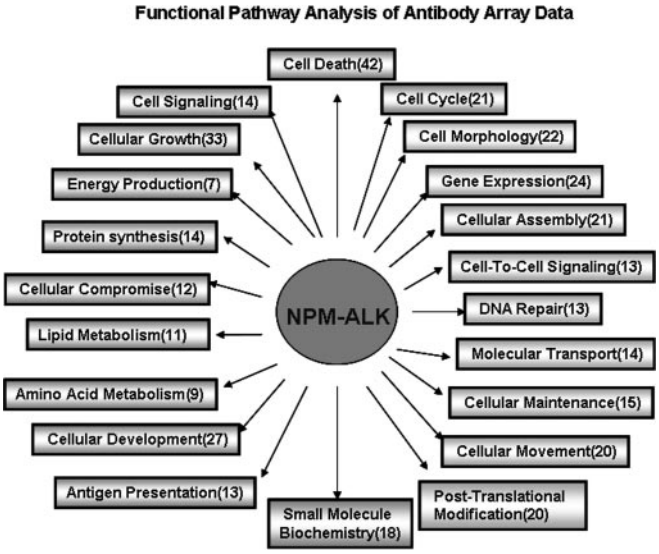

FIG. 5. **Functional pathway analysis of NPM-ALK-induced differentially expressed proteins (antibody microarray data).** The Ingenuity Pathway Analysis software was used to analyze the functional pathways of the NPM-ALK-induced differentially expressed proteins identified by antibody microarray. The numbers in parentheses represent the number of proteins belonging to the corresponding pathways.

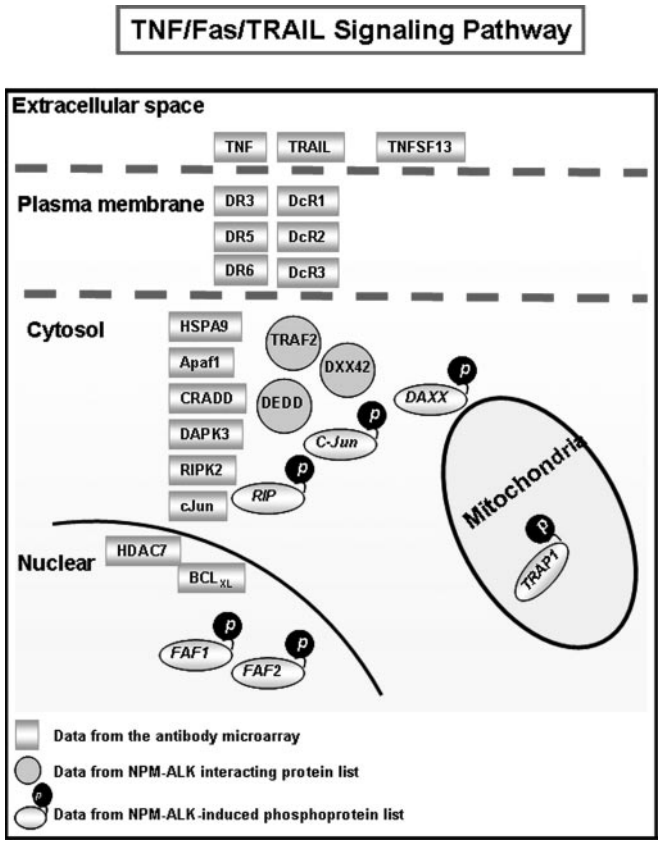

FIG. 6. **Schematic representation of TNF/Fas/TRAIL signaling pathway.** By analyzing our proteomics data, antibody microarray data, and our previously published binding protein data (20), a number of signaling pathways were identified, and the TNF/Fas/TRAIL signaling pathway is highlighted here. DEDD: Death effector domain-containing protein; DAXX: Death domain-associated protein 6.

phosphoproteins provided in supplemental Table S1. First of all, only a few proteins were validated, ultimately resulting in some novel insight into NPM-ALK-mediated lymphomagenesis (see below). For the remaining proteins, validation work is required if anyone is interested in taking the leads from the protein list to do biological studies, *e.g.* investigating other NPM-ALK-modulated signaling pathways. Second, this list was generated not only just once but also under the conditions used where the phosphoproteome reflected the status of a wide range of cellular states (*e.g.* cell growth was not synchronized). The presence of a phosphopeptide in the list provides the evidence of its existence, whereas the absence of the phosphopeptide in the list does not mean it is non-existent in the proteins expressed in the cells. Third, we cannot exclude the possibility that the presence or absence of a phosphopeptide or phosphoprotein is the result of the change in the protein expression level. Fourth, although the expression level of NPM-ALK and phosphorylation levels of several downstream proteins in GP293 cells transfected with either *NPM-ALK* or *NPM-ALK^{FFF}* were found to be similar to those of ALK^{+} ALCL cells (see above), we could not rule out completely the possibility of an un-natural expression level of the kinase that may affect the phosphoproteome profiles. Thus, this list should only serve as the

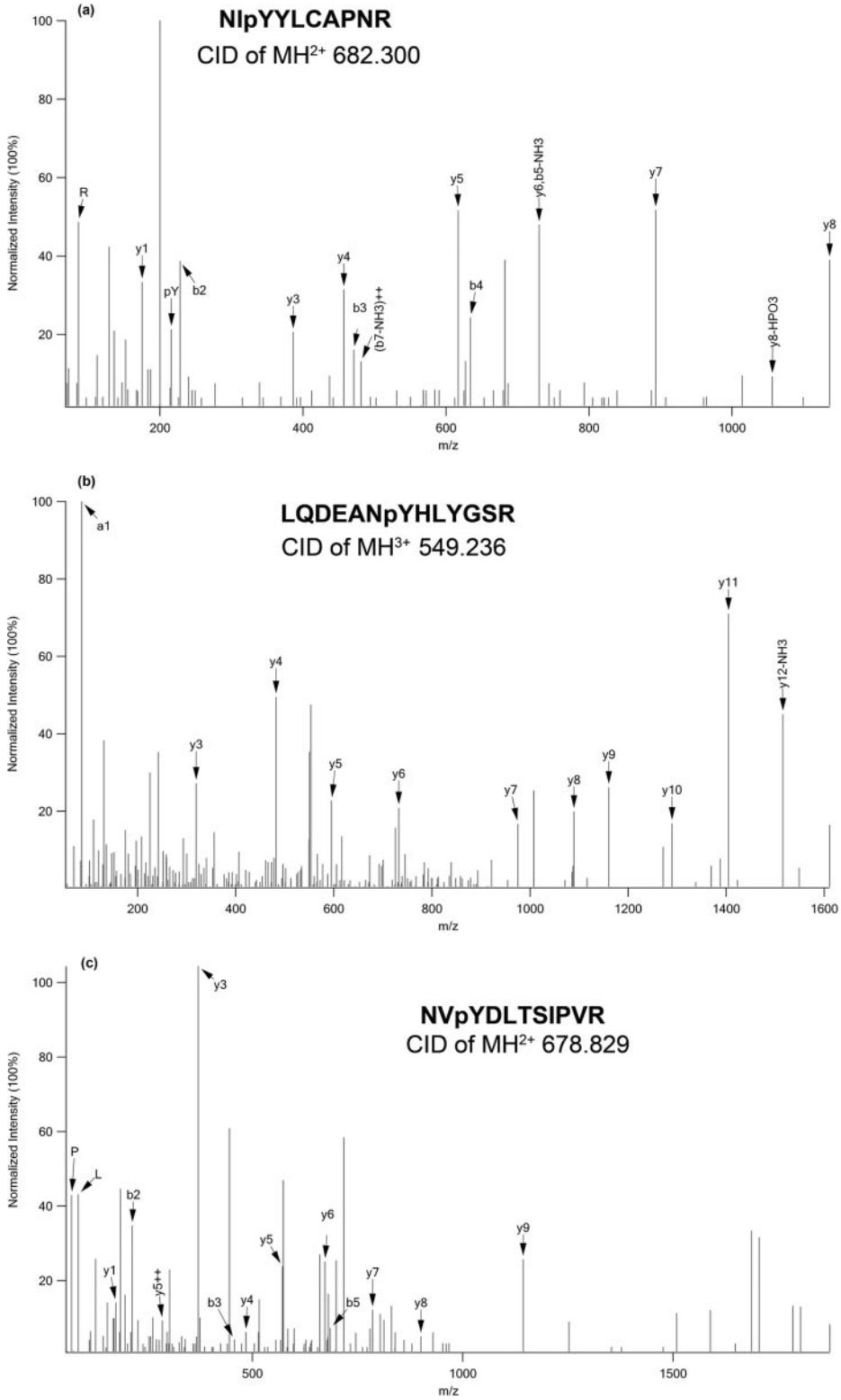

FIG. 7. **Representative MS/MS spectra of phosphopeptides from three proteins in TNF/Fas/TRAIL pathway: TRAP1 (*a*), RIP (*b*), and FAF1 (*c*).**

entry point for generating a hypothesis for further biological validation.

Bioinformatics Analysis—Using the Ingenuity Pathway Analysis software, we determined whether the 506 phosphoproteins can be grouped into canonical functional cellular pathways. The results are illustrated in Fig. 4; details are included in supplemental Table S2. The pathways to which the highest number of phosphoproteins belong are cell death

TABLE I

Identification of known NPM-ALK substrates in phosphoprotein list generated from this work

X, previously reported NPM-ALK-induced phosphoproteins that were identified exclusively in the *NPM-ALK*-transfected GP293 cells.

Swiss-Prot ID	Protein name	Identified	Ref.	Swiss-Prot ID	Protein name	Identified	Ref.
P40763	STAT3	X	41, 71	P28482	ERK2	X	14
P29353	SHC-transforming protein 1 (SHC)	X	72	Q86WB0	NIPA[a]	X	19
P50552	Vasodilator-stimulated phosphoprotein	X	16	P31939	Bifunctional purine biosynthesis protein PURH (ATIC)		16
Q06124	Tyrosine-protein phosphatase non-receptor type 11 (SHP2)	X	73	Q60674	Tyrosine-protein kinase JAK2		74
P19174	Phospholipase C-γ-1	X	40	P42229	Signal transducer and activator of transcription 5A (STAT5)		75
P48736	PI3K subunit p110	X	9	Q14103	Heterogeneous nuclear ribonucleoprotein D0 (AUF1)		76
P12931	p60-Src[a]	X	77	P35568	Insulin receptor substrate 1 (IRS-1)		72
P05412	Proto-oncogene c-Jun	X	18	P31749	AKT		9
P23246	PTB-associated-splicing factor (PSF)	X	78	Q9UQC2	Growth factor receptor-bound protein 2-associated protein 2 (Gab-2)	X	73
P27361	Extracellular signal-regulated kinase 1 (p44-ERK1)	X	14	Q9UKW4	Guanine nucleotide exchange factor VAV3		79
P08069	Insulin-like growth factor 1 receptor		80	P42345	mTOR	X	12

[a] Previously reported NPM-ALK-induced phosphoproteins that were identified in both *NPM-ALK*- and *NPM-ALK^{FFF}* mutant-transfected GP293 cells.

TABLE II

Proteins known to be NPM-ALK-interacting protein that were also found in phosphoprotein list generated from this work

Swiss-Prot ID	Protein name	Swiss-Prot ID	Protein name
O00170	Aryl hydrocarbon receptor-interacting protein (AIP)	Q15648	Mediator of RNA polymerase II transcription subunit 1 (MED1)
O14976	GAK	Q16543	Hsp90 co-chaperone Cdc37 (CDC37)
O15226	Transcription factor NRF (NKRF)*	Q5SRE5	Nucleoporin NUP188 homolog (NUP188)
P05198	EIF-2α (IF2A)	Q5T6F2	Ubiquitin-associated protein 2 (UABP2)
P05412	Proto-oncogene c-Jun (JUN)[a]	Q86YZ3	Hornerin (HORN)
P10809	Heat shock protein 60 (CH60)	Q99961	SH3 domain-containing GRB2-like protein 1 (SH3G1)
P12270	Nucleoprotein TPR (TPR)	Q9HD20	Probable cation-transporting ATPase 13A1 (AT131)
P29353	SHC-transforming protein 1 (SHC)[a]	Q9NNW5	WD repeat-containing protein 6 (WDR6)
P46060	Ran GTPase-activating protein 1 (RanGAP1)	Q9NQT8	Kinesin-like protein KIF13B (KI13B)
P61289	Proteasome activator 28 subunit γ (PSME3)	Q9P0L0	Vesicle-associated membrane protein-associated protein A (VAPA)[a]
Q00341	High density lipoprotein-binding protein (VIGLN)**	Q9UGP4	LIM domain-containing protein 1 (LIMD1)

[a] Represents the previously reported NPM-ALK-induced phospho-binding partner (20). *NKRF: NF-kappa-B-repressing factor. **VIGLN: Vigilin.

(n = 122), cell growth (n = 98), gene expression regulation (n = 95), cell morphology (n = 82), and cell cycle (n = 77). Specifically, we found signatures of several cellular signaling pathways that have been previously shown to be modulated by NPM-ALK, including those of PI3K/AKT, JAK/STAT3, and ERK/MAPK (supplemental Table S3). Importantly, our analysis also highlighted a number of cellular pathways/processes that have not been described in association with NPM-ALK. These included actin cytoskeleton signaling (n = 15), integrin signaling (n = 14), interleukin signaling (n = 13), apoptosis (n = 13), and glucocorticoid receptor signaling (n = 12).

To provide further evidence that cellular pathways/processes are modulated by NPM-ALK, we used a large scale antibody array to compare GP293 cells expressing NPM-ALK and cells expressing NPM-ALK^{FFF}. As shown in Table III, we found evidence of statistically significant changes in the expression of the genes of 56 proteins (of a total of 725 in the array). We then analyzed these 56 proteins using the Ingenuity Pathway Analysis software, and we found that most of these proteins are involved in cell death (n = 42), cell growth (n = 33), cell cycle (n = 21), and cell signaling (n = 14). The E3 ubiquitin proteasome degradation pathway was also highlighted as there were eight E3 ubiquitination ligases that were found to be phosphorylated, including ZNRF2, RFFL, TOPRS, RN19A, TRIM133, MGRN1, RNF8, and HERC1. Of great interest, we also found a substantial overlap of the involved

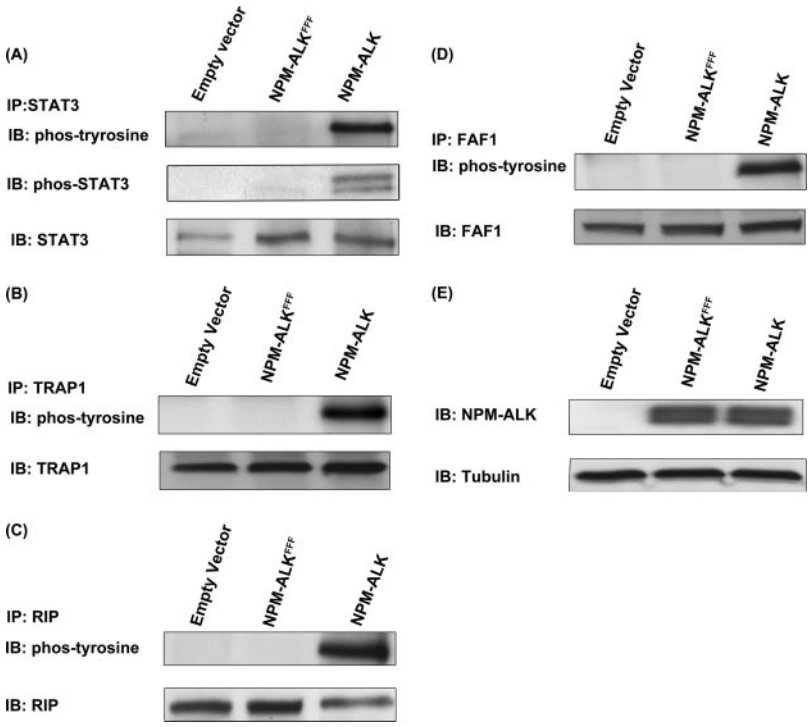

FIG. 8. **Validation of phosphoproteins involved in TNF/Fas/TRAIL signaling pathway using GP293 cells transfected with empty vector, *NPM-ALK^{FFF}* mutant, and *NPM-ALK*.** The immunoprecipitation (*IP*) experiments were performed using empty vector-, *NPM-ALK^{FFF}* mutant-, and *NPM-ALK*-transfected GP293 cell with anti-STAT3 antibody (*A*), anti-TRAP1 antibody (*B*), anti-RIP antibody (*C*), and anti-FAF1 antibody (*D*). The phosphorylation statuses of these four proteins were detected by using anti-phosphotyrosine antibody. *E*, the presence of NPM-ALK was detected in lysates from empty vector-, *NPM-ALK^{FFF}* mutant-, and *NPM-ALK*-transfected cells. *IB*, immunoblot; *phos*, phospho.

signal pathways between proteomics data (Fig. 4) and antibody array data (Fig. 5). One of the overlapping pathways that has not been reported previously in association with NPM-ALK is that of the TNF/Fas/TRAIL signaling pathway. Specifically, using the antibody microarray, we found that six TNF receptors (DR5, DR3, DR6, DcR1, DcR2, and DcR3) and two components of the TNF complex (DAPK3 and CRADD) were significantly up-regulated in the *NPM-ALK*-transfected GP293 cells (Fig. 6). Based on our proteomics data (supplemental Table S1), three TNF signaling molecules (RIP, TRAP1, and FAF1) were identified. All three were phosphorylated at the tyrosine residues. Fig. 7 shows the fragment ion spectra of phosphopeptides from RIP, TRAP1, and FAF1 generated by the Q-TOF mass spectrometer with peak assignments.

Identification of Known NPM-ALK Substrates—As summarized in Table I, we identified a total of 22 proteins (seven phosphotyrosine and 15 phosphoserine/phosphothreonine) that were previously reported to be phosphorylated by NPM-ALK. We found 14 of these 22 proteins on our list, and they included STAT3, SHC, SHP2, mTOR, phospholipase C γ, PI3K, Src, ERK1, ERK2, vasodilator-stimulated phosphoprotein, PTB-associated splicing factor, NIPA, and growth factor receptor-bound protein 2-associated protein 2 (Gab2). In contrast, eight were not found, and they included JAK2, STAT5, AKT, heterogeneous nuclear ribonucleoprotein D0 (AUF1), guanine nucleotide exchange factor VAV3; insulin-like growth factor receptor, and bifunctional purine biosynthesis protein PURH (ATIC).

Identification of Known NPM-ALK-interacting Proteins—We then assessed which of these 506 proteins are also known to be proteins physically associated with NPM-ALK. Thus, we compared these proteins with our previously published data (20), which identified 254 proteins as potential NPM-ALK binding partners. Twenty-two NPM-ALK-induced phosphoproteins were also previously found to be the binding partners of NPM-ALK (Table II). With the exception of three proteins (SHC, vesicle-associated membrane protein-associated protein A (VAPA), and c-Jun), none of these proteins have been previously described to be phosphorylated or bound by NPM-ALK. A number of these proteins, including PSME3, MED1, cyclin G-associated kinase (GAK), WDR6, NRF, TPR, and NUP188, are known to have important biological roles, such as gene transcription (53, 54), cell cycle (55–57), and cellular transport (58).

Validation of Phosphoproteins Involved in TNF/Fas/TRAIL Pathway—Considering the biological importance of the TNF/Fas/TRAIL signaling pathway and the fact this pathway has not been previously described in the context of NPM-ALK, we decided to further confirm the tyrosine phosphorylation of the three proteins revealed by our proteomics studies, namely RIP, TRAP1, and FAF1, using immunoprecipitation. First, validation experiments were performed using GP293 cells transfected with *NPM-ALK*, *NPM-ALK^{FFF}* mutant, and empty vector. STAT3 was included as a positive control. As shown in Fig. 8, all three proteins were phosphorylated only in the presence of NPM-ALK. The immunoblots were probed with anti-phosphotyrosine antibody. Second, to document their biological relevance in ALK$^+$ ALCL, we used Karpas 299 and SU-DH-L1, two well studied ALK$^+$ ALCL cell lines, to detect the expression and the phosphorylation statuses of RIP, TRAP1, and FAF1. As shown in Fig. 9, all three proteins were

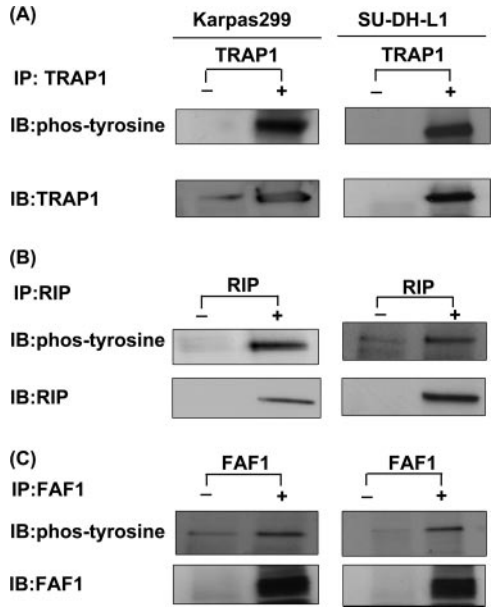

FIG. 9. **Validation of phosphoproteins involved in TNF/Fas/TRAIL signaling pathway using ALK$^+$ ALCL cell lines.** The immunoprecipitation (*IP*) experiments were performed using Karpas 299 and SU-DH-L1, two well studied ALK$^+$ ALCL cell lines, with anti-TRAP1 antibody (*A*), anti-RIP antibody (*B*), and anti-FAF1 antibody (*C*). The phosphorylation statuses of these three proteins were detected by using anti-phosphotyrosine antibody. The immunoprecipitation experiments without antibody were used as control experiments. *IB*, immunoblot; *phos*, phospho.

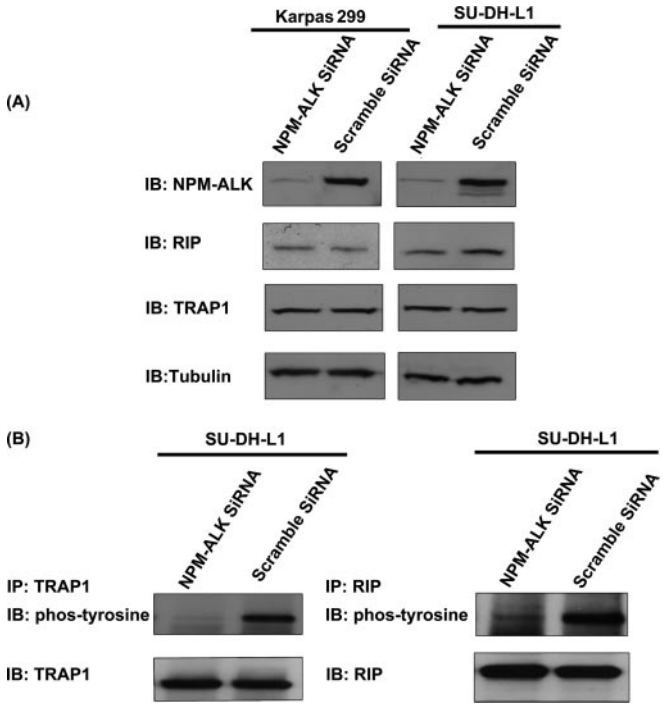

FIG. 10. **Phosphorylation statuses of TRAP1 and RIP in NPM-ALK knockdown ALK$^+$ ALCL cells.** *A*, NPM-ALK siRNA was used to decrease the expression level of NPM-ALK in SU-DH-L1 cells. The scrambled siRNA-transfected SU-DH-L1 was used as a negative control. The expression of NPM-ALK was detected by using anti-ALK antibody. The expression levels of TRAP1 and RIP were detected using anti-TRAP antibody and anti-RIP antibody, respectively. *B*, immunoprecipitation (*IP*) experiments were performed using NPM-ALK knockdown SU-DH-L1 with anti-TRAP1 antibody and anti-RIP antibody, respectively. The phosphorylation statuses of TRAP1 and RIP were detected using anti-phosphotyrosine antibody. The scrambled siRNA-transfected SU-DH-L1 cell lysates were used as controls. *IB*, immunoblot; *phos*, phospho.

expressed and phosphorylated in two of two examined ALK$^+$ ALCL cell lines. Lastly, to further confirm the role of NPM-ALK in phosphorylating TRAP1 and RIP in ALK$^+$ ALCL cells, we used NPM-ALK siRNA to knock down NPM-ALK of SU-DH-L1 and examined the phosphorylation statuses of TRAP1 and RIP. Fig. 10 shows that siRNA significantly down-regulated the expression level of NPM-ALK in these two ALK$^+$ ALCL cell lines; this in turn led to the loss of phosphorylation of TRAP1 and RIP. The expression level of TRAP1 and RIP was hardly affected after knockdown of NPM-ALK.

Knockdown of TRAP1 Facilitates TRAIL-induced Cell Death—To determine the functional role of the TNF/Fas/TRAIL pathway in the survival of ALK$^+$ ALCL, we selected one biologically relevant protein, namely TRAP1. We then compared the cell viability of TRAP1 knockdown SU-DH-L1 with that of scrambled siRNA-transfected SU-DH-L1 after treatment with TRAIL. Fig. 11*A* shows the substantial decrease of the expression level of TRAP1. As illustrated in Fig. 11*B*, the cell viability assay indicated that knockdown of TRAP1 sensitized TRAIL-induced cell death (about 30% reduction by 100 ng/ml TRAIL) ($p < 0.05$). The number of TRAIL-induced dead cells were further evaluated by using trypan blue staining and showed a significant increase after knockdown of TRAP1 of SU-DH-L1 ($p < 0.05$) (Fig. 11*D*).

Knockdown of TRAP1 Facilitates Doxorubicin-induced Cell Death—Considering the biological importance of TRAP1, we further investigated the potential effect of knockdown of TRAP1 on the antitumor activity of doxorubicin, a chemotherapeutic drug widely used in the clinic for treatment of ALK$^+$ ALCL patients. Fig. 11*C* illustrates that doxorubicin treatment showed a significant decrease of cell viability against TRAP1 knockdown SU-DH-L1 cells (about 53% reduction by 200 nM doxorubicin) ($p < 0.05$). The half-maximal inhibitory concentration (IC_{50}) of doxorubicin for control SU-DH-L1 is 444.1 nM, whereas the IC_{50} of doxorubicin for TRAP1 knockdown SU-DH-L1 is 132.3 nM, which shows a significant difference ($p < 0.0001$). Moreover, using trypan blue staining, the number of doxorubicin-induced dead cells was evaluated and showed a significant increase after knockdown of TRAP1 of SU-DH-L1 ($p < 0.05$) (Fig. 11*D*).

DISCUSSION

In this study, we used a proteomics method, together with a functional validation, to identify novel signaling molecules downstream of NPM-ALK. Due to the enrichment of low abundance phosphotyrosine peptides, the proportion of phospho-

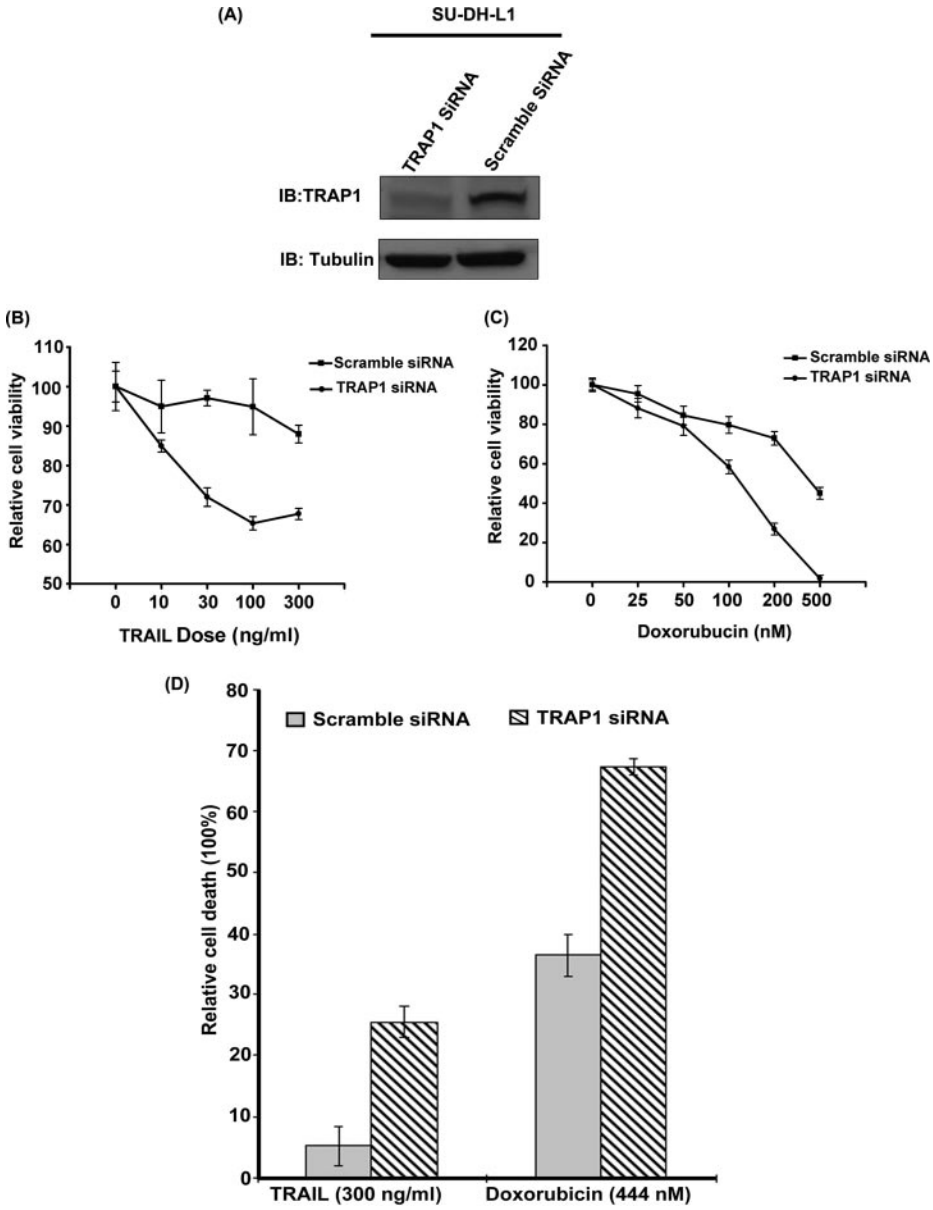

FIG. 11. **Knockdown of TRAP1 facilitated TRAIL- or doxorubicin-induced cell death.** *A*, TRAP1 siRNA was used to decrease the expression level of TRAP1 in SU-DH-L1 cells. The scrambled siRNA-transfected SU-DH-L1 was used as a negative control. The expression level of TRAP1 was detected by Western blot. *B*, TRAP1 knockdown SU-DH-L1 and scrambled siRNA-transfected SU-DH-L1 were treated with TRAIL in a dose-dependent manner, respectively. As shown here, scrambled siRNA-transfected SU-DH-L1 cells were resistant to TRAIL-induced cell death, whereas knockdown of TRAP1 sensitized SU-DH-L1 to TRAIL-induced cell death. *C*, TRAP1 knockdown SU-DH-L1 and scrambled siRNA-transfected SU-DH-L1 were treated with the chemotherapy drug doxorubicin in a dose-dependent manner, respectively. The results showed that knockdown of TRAP1 enhanced chemotherapy drug doxorubicin-induced cell death. *D*, the number of TRAIL- (300 ng/ml) or doxorubicin (444 nM)-induced dead cells were evaluated using Coomassie Blue staining. It showed that the number of TRAIL- or doxorubicin-induced dead cells significantly increased after knockdown of TRAP1 of SU-DH-L1 ($p < 0.05$). *IB*, immunoblot. The error bar represents a standard deviation of the replicates.

tyrosine-carrying proteins in this study was 25%. Detection of this high proportion of phosphotyrosine peptides most likely reflects the activated oncogenic tyrosine kinase property of NPM-ALK. NPM-ALK induces phosphorylation profile changes especially in the tyrosine phosphorylation profile. However, we cannot completely rule out the possibility of a significant loss of phosphoserine or phosphothreonine peptides during the sample workup. The purity of phosphopeptides after enrichment was about 70% in our work; this level is consistent with previous reports (59–61).

Because of the differences in the phosphopeptide enrichment protocol as well as other technical differences, some discrepancies between the results of the two previous studies of NPM-ALK (16, 17) and ours were observed (*e.g.* we additionally identified >300 NPM-ALK-induced phosphoproteins carrying phosphoserine and phosphothreonine). In contrast with the other two studies, we used GP293 cells transfected with *NPM-ALK*. We do consider the possibility that by using immortalized cells we avoided missing important proteins downstream of NPM-ALK whose expression may have been aberrantly silenced in cancerous cell lines. Because GP293 is an embryonic kidney cell line, it is perceivable that the phosphoproteomic changes induced by NPM-ALK will differ somewhat from those seen in T cells of mature immunophenotype. Nevertheless, one of the key advantages of using this *in vitro* system is that we had the opportunity to create a negative control (*i.e.* GP293 cells transfected with the *NPM-ALK*^{FFF} mutant), which improved the specificity of our results. Another advantage is related to the fact that NPM-ALK is absent in untransfected GP293 cells, and therefore, the specificity of

TABLE III

Antibody array data showing differentially expressed proteins induced by NPM-ALK

W/F, wild type/FFF mutant; MAP, mitogen-activated protein.

Symbol	Protein name	Ratio (W/F)	Symbol	Protein name	Ratio (W/F)
Peptidase					
ADAM17	Disintegrin and metalloproteinase domain-containing protein 17	2.08	Caspase13	Caspase 13, apoptosis-related cysteine peptidase	2.17
CTSD	Cathepsin D	2.17			
Cytokine					
TNFSF13	Tumor necrosis factor (ligand) superfamily, member 13 (APRIL)	2.20	TNF	Tumor necrosis factor (TNF superfamily, member 2)	13.75
TNFSF10	Tumor necrosis factor (ligand) superfamily, member 10 (TRAIL)	3.00			
Enzyme					
OGT	*O*-Linked *N*-acetylglucosamine (GlcNAc) transferase	2.35	RRM2B	Ribonucleotide reductase M2 B (TP53-inducible)	2.73
DNASE2A	Deoxyribonuclease II, lysosomal	2.58			
Kinase					
CSNK2B	Casein kinase 2, β polypeptide	2.28	MAPK1	Mitogen-activated protein kinase 1 (ERK2)	2.12
RIPK2	Receptor-interacting serine-threonine kinase 2	12.49	MAP2K3	Mitogen-activated protein kinase kinase 3	21.56
DAPK3	Death-associated protein kinase 3	3.53	STK17A	Serine/threonine kinase 17a	2.36
CDK3	Cyclin-dependent kinase 3	2.05	PRKCB	Protein kinase C, β	2.51
Transcription regulator					
HDAC7	Histone deacetylase 7	3.37	JUN	Jun oncogene	2.30
MTA2	Metastasis-associated 1 family, member 2	2.26	TSG101	Tumor susceptibility gene 101	2.76
Sirt1	Sirtuin (silent mating type information regulation 2 homolog) 1	2.26	RYBP	RING1- and YY1-binding protein	2.35
c-Myc	Myelocytomatosis viral oncogen homolog	2.18	RND3	Rho family GTPase 3	2.40
Transmembrane receptor					
TNFRSF10C	Tumor necrosis factor receptor superfamily, member 10c (DcR1)	2.40	TNFRSF10D	Tumor necrosis factor receptor superfamily, member 10d (DcR2)	2.34
TNFRSF6B	Tumor necrosis factor receptor superfamily, member 6b (DcR3)	2.57	TNFRSF25	Tumor necrosis receptor superfamily, member 25 (DR3)	2.61
TNFRSF10B	Tumor necrosis factor receptor superfamily, member 10b (DR5)	2.39	TNFRSF21	Tumor necrosis factor superfamily member 21 (DR6)	3.10
Growth factor					
TGFB1	Transforming growth factor, β1	2.23			
Transporter					
SYT1	Synaptotagmin I	2.03			
Others					
HSPA9	Heat shock 70-kDa protein 9 (mortalin)	2.45	H3F3A	H3 histone, family 3A	3.08
MADD	MAP kinase-activating death domain	3.11	MAP1B	Microtubule-associated protein 1B	2.24
MTBP	Mdm2, transformed 3T3 cell double minute 2, p53-binding protein (mouse)-binding protein, 104 kDa	2.74	MYD88	Myeloid differentiation primary response gene (88)	2.02
Ppp1r9a	Protein phosphatase 1, regulatory subunit 9A	3.20	PPP1R9B	Protein phosphatase 1, regulatory subunit 9b	2.64
PERP	PERP, TP53 apoptosis effector	3.51	BBC3	BCL2 binding component 3	3.01
CRADD	CASP2 and RIPK1 domain-containing adaptor with death domain	15.29	MAPT	Microtubule-associated protein tau	5.35
IFRD1	Interferon-related developmental regulator 1	2.01	CCND1	Cyclin D1	2.49
APAF1	Apoptotic peptidase activating factor 1	2.27	BID	BH3-interacting domain death agonist	2.06
BCL2L1	BCL2-like 1	3.29			

our results was further improved. Our previous publication (20) has demonstrated that >80% of the proteins bound to the NPM-ALK ectopically expressed in GP293 cells also can be found in ALK$^+$ ALCL cells. In addition, our results have shown that the expression levels of NPM-ALK in the *NPM-ALK*-transfected GP293 and ALK$^+$ ALCL cell lines are not dramatically different, and the phosphorylation level of known downstream targets of NPM-ALK (*e.g.* STAT3, SHC, Src, and ERK1/2) in both systems is similar, also strongly suggesting that GP293 cells are a valid *in vitro* model for NPM-ALK studies.

The validity of our results is supported by the following findings. First, most of the previously known signaling pathways implicated in NPM-ALK pathobiology were detected by our method, and they include the PI3K/AKT signaling pathway, JAK/STAT3 pathway, ERK/MAPK pathway, and JNK/c-Jun pathway. Second, a comparison between the results of this study and those of the two previous studies revealed 45 phosphoproteins found in one or both of these two previous studies of NPM-ALK, representing ~56% of the total phosphoproteins carrying phosphotyrosine (*i.e.* a total of 126 proteins found in our studies) (supplemental Table S5). Third, 41 of the phosphoproteins overlap with those of previously reported NPM-ALK substrates and/or previously reported NPM-ALK-interacting proteins. Fourth, in the TNF/Fas/TRAIL pathway, we validated the tyrosine phosphorylation of three proteins in both *NPM-ALK*-transfected GP293 cells and ALK^+ ALCL cells. Lastly, of those 506 NPM-ALK-induced phosphoproteins, all the phosphopeptides were identified with a confidence level of >95%. Each of their MS/MS spectra and phosphorylation sites were also manually examined.

We carried out the protein microarray analysis to further evaluate the expression level changes of a number of proteins involved in several crucial signal pathways, including cell death, cell growth, and cell cycle (Table III). Although these data may be interpreted that the presence or absence of a phosphopeptide could simply be the consequence of increased expression of the general protein level, the modification of these important signal pathways by NPM-ALK was suggested by both the antibody microarray data and the MS data. However, at present, it is technically impossible to use this approach to validate all of the proteins revealed by the MS, considering that the antibody microarray covers only a small portion of the proteins detected from the MS data.

To our knowledge, NPM-ALK has never been reported to be associated with the TNF/Fas/TRAIL signaling pathway. Dysregulation of TNF/Fas/TRAIL signaling pathway is strongly associated with tumorigenesis due to antiapoptosis and cell growth-promoting effects (62–65). In this study, the TNF/Fas/TRAIL signaling pathway was found to be highly modulated by NPM-ALK with involvement at all stages of the pathway. Of note, our previously published results of NPM-ALK-interacting proteins (20) showed that three adaptor proteins (*i.e.* TRAF2, DEDD, and DDX42) involved in the TNF/Fas/TRAIL signaling were bound to NPM-ALK (see Fig. 6), and these findings strengthen our argument that NPM-ALK modulates this pathway. The majority of the identified TNF signaling molecules (*i.e.* RIP, FAF1, and TRAP1) were those known to play an important role in regulating apoptosis. They were further validated in *NPM-ALK*-transfected GP293 as well as ALK^+ ALCL cells. More importantly, the phosphorylation of RIP and TRAP1 was confirmed to be directly associated with NPM-ALK using NPM-ALK siRNA. This is the first demonstration that NPM-ALK induced the phosphorylation of TRAP1 at Tyr^{499} and RIP at Tyr^{384}. We further examined the expression levels of TRAP1 and RIP after NPM-ALK knockdown, showing that the expression levels of TRAP1 and RIP were not affected by NPM-ALK. These two proteins were previously reported to suppress apoptosis and promote cell growth (66–69). In particular, RIP has been reported to be involved in TNF receptor-mediated induction of cell survival through both the inhibition of caspase 8-initiated apoptosis and the promotion NF-κB-induced cell growth (66, 67). The phosphorylation at Tyr^{384} (same as our data) of RIP has been reported previously, but its function has not been explored (70). TRAP1 (68) has been reported to play an important role in the suppression of apoptosis through the inhibition of cytochrome *c* release from mitochondria under oxidative stress (69). To further investigate the role of TRAP1 in ALK-mediated lymphomagenesis, we analyzed the biological function of TRAP1 in the survival of ALK^+ ALCL cells treated with TRAIL or doxorubicin. Interestingly, TRAP1 knockdown was shown to sensitize both TRAIL and doxorubicin-induced cell death. Our data indicated the importance of TRAP1 in mediating tumor sensitivity to both TRAIL and doxorubicin treatment and its valuable role for the design of new therapeutic strategies. Although the direct link between the phosphorylation of TRAP1 (induced by NPM-ALK) and NPM-ALK-induced tumorigenesis has not been established, we would like to point out that, because of this study, we can now focus on the potential of TRAP1 phosphorylation-induced tumorigenesis. Currently, we are performing further functional analysis of phosphorylated TRAP1 and RIP in ALK^+ ALCL.

In conclusion, our study identified a set of proteins downstream of NPM-ALK that contribute to the maintenance of neoplastic phenotype using our phosphoproteomics analysis strategy. We believe that our improved understanding of ALK^+ ALCL pathobiology has important implications for the development of novel therapeutic strategies.

Acknowledgments—We thank Peter Kaiser (University of California Irvine) for providing the HB-tagged vector, Dr. Stephen W. Morris for providing the NPM-ALK cDNA plasmid, and Dr. Robert J. Ingham for technical help on transfection.

* This work was supported by operating research grants from the Alberta Cancer Foundation and Canadian Institute for Health Research (to R. L.) and the Natural Sciences and Engineering Research Council of Canada and the Canada Research Chairs Program (to L. L.).

[S] This article contains supplemental Tables S1–S5.

‖ Both authors contributed equally to this work.

** To whom correspondence may be addressed. Tel.: 780-432-8457; Fax: 780-432-8214; E-mail: rlai@ualberta.ca, or Tel.: 780-492-3250; Fax: 780-492-8231; E-mail: liang.li@ualberta.ca.

REFERENCES

1. Delsol, G., Ralfkiaer, E., Stein, H., Wright, D., and Jaffe, E. (2001) *Pathology and Genetics Tumors of Haematopoietic and Lymphoid Tissues: World Health Organization Classification of Tumors*, IARC Press, Lyon, France
2. Stein, H., Foss, H. D., Dürkop, H., Marafioti, T., Delsol, G., Pulford, K., Pileri, S., and Falini, B. (2000) CD30(+) anaplastic large cell lymphoma: a

review of its histopathologic, genetic, and clinical features. *Blood* **96,** 3681–3695
3. Mason, D. Y., Bastard, C., Rimokh, R., Dastugue, N., Huret, J. L., Kristoffersson, U., Magaud, J. P., Nezelof, C., Tilly, H., Vannier, J. P., Hemet, J., and Warnke, R. (1990) CD30-positive large cell lymphomas ('Ki-1 lymphoma') are associated with a chromosomal translocation involving 5q35. *Br. J. Haematol.* **74,** 161–168
4. Morris, S. W., Kirstein, M. N., Valentine, M. B., Dittmer, K., Shapiro, D. N., Look, A. T., and Saltman, D. L. (1995) Fusion of a kinase gene, ALK, to a nucleolar protein gene, NPM, in non-Hodgkin's lymphoma. *Science* **267,** 316–317
5. Morris, S. W., Kirstein, M. N., Valentine, M. B., Dittmer, K. G., Shapiro, D. N., Saltman, D. L., and Look, A. T. (1994) Fusion of a kinase gene, ALK, to a nucleolar protein gene, NPM, in non-Hodgkin's lymphoma. *Science* **263,** 1281–1284
6. Benz-Lemoine, E., Brizard, A., Huret, J. L., Babin, P., Guilhot, F., Couet, D., and Tanzer, J. (1988) Malignant histiocytosis: a specific t(2;5)(p23;q35) translocation? Review of the literature. *Blood* **72,** 1045–1047
7. Fischer, P., Nacheva, E., Mason, D. Y., Sherrington, P. D., Hoyle, C., Hayhoe, F. G., and Karpas, A. (1988) A Ki-1 (CD30)-positive human cell line (Karpas 299) established from a high-grade non-Hodgkin's lymphoma, showing a 2;5 translocation and rearrangement of the T-cell receptor beta-chain gene. *Blood* **72,** 234–240
8. Bai, R. Y., Ouyang, T., Miething, C., Morris, S. W., Peschel, C., and Duyster, J. (2000) Nucleophosmin-anaplastic lymphoma kinase associated with anaplastic large-cell lymphoma activates the phosphatidylinositol 3-kinase/Akt antiapoptotic signaling pathway. *Blood* **96,** 4319–4327
9. Slupianek, A., Nieborowska-Skorska, M., Hoser, G., Morrione, A., Majewski, M., Xue, L., Morris, S. W., Wasik, M. A., and Skorski, T. (2001) Role of phosphatidylinositol 3-kinase-Akt pathway in nucleophosmin/anaplastic lymphoma kinase-mediated lymphomagenesis. *Cancer Res.* **61,** 2194–2199
10. Amin, H. M., McDonnell, T. J., Ma, Y., Lin, Q., Fujio, Y., Kunisada, K., Leventaki, V., Das, P., Rassidakis, G. Z., Cutler, C., Medeiros, L. J., and Lai, R. (2004) Selective inhibition of STAT3 induces apoptosis and G(1) cell cycle arrest in ALK-positive anaplastic large cell lymphoma. *Oncogene* **23,** 5426–5434
11. Kutok, J. L., and Aster, J. C. (2002) Molecular biology of anaplastic lymphoma kinase-positive anaplastic large-cell lymphoma. *J. Clin. Oncol.* **20,** 3691–3702
12. Marzec, M., Kasprzycka, M., Liu, X., El-Salem, M., Halasa, K., Raghunath, P. N., Bucki, R., Wlodarski, P., and Wasik, M. A. (2007) Oncogenic tyrosine kinase NPM/ALK induces activation of the rapamycin-sensitive mTOR signaling pathway. *Oncogene* **26,** 5606–5614
13. Gu, L., Gao, J., Li, Q., Zhu, Y. P., Jia, C. S., Fu, R. Y., Chen, Y., Liao, Q. K., and Ma, Z. (2008) Rapamycin reverses NPM-ALK-induced glucocorticoid resistance in lymphoid tumor cells by inhibiting mTOR signaling pathway, enhancing G1 cell cycle arrest and apoptosis. *Leukemia* **22,** 2091–2096
14. Marzec, M., Kasprzycka, M., Liu, X., Raghunath, P. N., Wlodarski, P., and Wasik, M. A. (2007) Oncogenic tyrosine kinase NPM/ALK induces activation of the MEK/ERK signaling pathway independently of c-Raf. *Oncogene* **26,** 813–821
15. Turner, S. D., Yeung, D., Hadfield, K., Cook, S. J., and Alexander, D. R. (2007) The NPM-ALK tyrosine kinase mimics TCR signalling pathways, inducing NFAT and AP-1 by RAS-dependent mechanisms. *Cell. Signal.* **19,** 740–747
16. Boccalatte, F. E., Voena, C., Riganti, C., Bosia, A., D'Amico, L., Riera, L., Cheng, M., Ruggeri, B., Jensen, O. N., Goss, V. L., Lee, K., Nardone, J., Rush, J., Polakiewicz, R. D., Comb, M. J., Chiarle, R., and Inghirami, G. (2009) The enzymatic activity of 5-aminoimidazole-4-carboxamide ribonucleotide formyltransferase/IMP cyclohydrolase is enhanced by NPM-ALK: new insights in ALK-mediated pathogenesis and the treatment of ALCL. *Blood* **113,** 2776–2790
17. Rush, J., Moritz, A., Lee, K. A., Guo, A., Goss, V. L., Spek, E. J., Zhang, H., Zha, X. M., Polakiewicz, R. D., and Comb, M. J. (2005) Immunoaffinity profiling of tyrosine phosphorylation in cancer cells. *Nat. Biotechnol.* **23,** 94–101
18. Leventaki, V., Drakos, E., Medeiros, L. J., Lim, M. S., Elenitoba-Johnson, K. S., Claret, F. X., and Rassidakis, G. Z. (2007) NPM-ALK oncogenic kinase promotes cell-cycle progression through activation of JNK/cJun signaling in anaplastic large-cell lymphoma. *Blood* **110,** 1621–1630
19. Ouyang, T., Bai, R. Y., Bassermann, F., von Klitzing, C., Klumpen, S., Miething, C., Morris, S. W., Peschel, C., and Duyster, J. (2003) Identification and characterization of a nuclear interacting partner of anaplastic lymphoma kinase (NIPA). *J. Biol. Chem.* **278,** 30028–30036
20. Wu, F., Wang, P., Young, L. C., Lai, R., and Li, L. (2009) Proteome-wide identification of novel binding partners to the oncogenic fusion gene protein, NPM-ALK, using tandem affinity purification and mass spectrometry. *Am. J. Pathol.* **174,** 361–370
21. Ficarro, S. B., McCleland, M. L., Stukenberg, P. T., Burke, D. J., Ross, M. M., Shabanowitz, J., Hunt, D. F., and White, F. M. (2002) Phosphoproteome analysis by mass spectrometry and its application to Saccharomyces cerevisiae. *Nat. Biotechnol.* **20,** 301–305
22. Carrascal, M., Ovelleiro, D., Casas, V., Gay, M., and Abian, J. (2008) Phosphorylation analysis of primary human T lymphocytes using sequential IMAC and titanium oxide enrichment. *J. Proteome Res.* **7,** 5167–5176
23. Villén, J., Beausoleil, S. A., Gerber, S. A., and Gygi, S. P. (2007) Large-scale phosphorylation analysis of mouse liver. *Proc. Natl. Acad. Sci. U.S.A.* **104,** 1488–1493
24. Thingholm, T. E., Jørgensen, T. J., Jensen, O. N., and Larsen, M. R. (2006) Highly selective enrichment of phosphorylated peptides using titanium dioxide. *Nat. Protoc.* **1,** 1929–1935
25. Larsen, M. R., Thingholm, T. E., Jensen, O. N., Roepstorff, P., and Jørgensen, T. J. (2005) Highly selective enrichment of phosphorylated peptides from peptide mixtures using titanium dioxide microcolumns. *Mol. Cell. Proteomics* **4,** 873–886
26. Pinkse, M. W., Uitto, P. M., Hilhorst, M. J., Ooms, B., and Heck, A. J. (2004) Selective isolation at the femtomole level of phosphopeptides from proteolytic digests using 2D-NanoLC-ESI-MS/MS and titanium oxide precolumns. *Anal. Chem.* **76,** 3935–3943
27. Marcantonio, M., Trost, M., Courcelles, M., Desjardins, M., and Thibault, P. (2008) Combined enzymatic and data mining approaches for comprehensive phosphoproteome analyses: application to cell signaling events of interferon-gamma-stimulated macrophages. *Mol. Cell. Proteomics* **7,** 645–660
28. Trost, M., English, L., Lemieux, S., Courcelles, M., Desjardins, M., and Thibault, P. (2009) The phagosomal proteome in interferon-gamma-activated macrophages. *Immunity* **30,** 143–154
29. Trinidad, J. C., Specht, C. G., Thalhammer, A., Schoepfer, R., and Burlingame, A. L. (2006) Comprehensive identification of phosphorylation sites in postsynaptic density preparations. *Mol. Cell. Proteomics* **5,** 914–922
30. Oda, Y., Nagasu, T., and Chait, B. T. (2001) Enrichment analysis of phosphorylated proteins as a tool for probing the phosphoproteome. *Nat. Biotechnol.* **19,** 379–382
31. Simon, E. S., Young, M., Chan, A., Bao, Z. Q., and Andrews, P. C. (2008) Improved enrichment strategies for phosphorylated peptides on titanium dioxide using methyl esterification and pH gradient elution. *Anal. Biochem.* **377,** 234–242
32. Salomon, A. R., Ficarro, S. B., Brill, L. M., Brinker, A., Phung, Q. T., Ericson, C., Sauer, K., Brock, A., Horn, D. M., Schultz, P. G., and Peters, E. C. (2003) Profiling of tyrosine phosphorylation pathways in human cells using mass spectrometry. *Proc. Natl. Acad. Sci. U.S.A.* **100,** 443–448
33. Munton, R. P., Tweedie-Cullen, R., Livingstone-Zatchej, M., Weinandy, F., Waidelich, M., Longo, D., Gehrig, P., Potthast, F., Rutishauser, D., Gerrits, B., Panse, C., Schlapbach, R., and Mansuy, I. M. (2007) Qualitative and quantitative analyses of protein phosphorylation in naive and stimulated mouse synaptosomal preparations. *Mol. Cell. Proteomics* **6,** 283–293
34. Smolka, M. B., Albuquerque, C. P., Chen, S. H., Schmidt, K. H., Wei, X. X., Kolodner, R. D., and Zhou, H. (2005) Dynamic changes in protein-protein interaction and protein phosphorylation probed with amine-reactive isotope tag. *Mol. Cell. Proteomics* **4,** 1358–1369
35. McNulty, D. E., and Annan, R. S. (2008) Hydrophilic interaction chromatography reduces the complexity of the phosphoproteome and improves global phosphopeptide isolation and detection. *Mol. Cell. Proteomics* **7,** 971–980
36. Ballif, B. A., Carey, G. R., Sunyaev, S. R., and Gygi, S. P. (2008) Large-scale identification and evolution indexing of tyrosine phosphorylation sites from murine brain. *J. Proteome Res.* **7,** 311–318

37. Zheng, H., Hu, P., Quinn, D. F., and Wang, Y. K. (2005) Phosphotyrosine proteomic study of interferon alpha signaling pathway using a combination of immunoprecipitation and immobilized metal affinity chromatography. *Mol. Cell. Proteomics* **4,** 721–730
38. Zhang, Y., Wolf-Yadlin, A., Ross, P. L., Pappin, D. J., Rush, J., Lauffenburger, D. A., and White, F. M. (2005) Time-resolved mass spectrometry of tyrosine phosphorylation sites in the epidermal growth factor receptor signaling network reveals dynamic modules. *Mol. Cell. Proteomics* **4,** 1240–1250
39. Boersema, P. J., Foong, L. Y., Ding, V. M., Lemeer, S., van Breukelen, B., Philp, R., Boekhorst, J., Snel, B., den Hertog, J., Choo, A. B., and Heck, A. J. (2010) In-depth qualitative and quantitative profiling of tyrosine phosphorylation using a combination of phosphopeptide immunoaffinity purification and stable isotope dimethyl labeling. *Mol. Cell. Proteomics* **9,** 84–99
40. Bai, R. Y., Dieter, P., Peschel, C., Morris, S. W., and Duyster, J. (1998) Nucleophosmin-anaplastic lymphoma kinase of large-cell anaplastic lymphoma is a constitutively active tyrosine kinase that utilizes phospholipase C-gamma to mediate its mitogenicity. *Mol. Cell. Biol.* **18,** 6951–6961
41. Zamo, A., Chiarle, R., Piva, R., Howes, J., Fan, Y., Chilosi, M., Levy, D. E., and Inghirami, G. (2002) Anaplastic lymphoma kinase (ALK) activates Stat3 and protects hematopoietic cells from cell death. *Oncogene* **21,** 1038–1047
42. Tartari, C. J., Gunby, R. H., Coluccia, A. M., Sottocornola, R., Cimbro, B., Scapozza, L., Donella-Deana, A., Pinna, L. A., and Gambacorti-Passerini, C. (2008) Characterization of some molecular mechanisms governing autoactivation of the catalytic domain of the anaplastic lymphoma kinase. *J. Biol. Chem.* **283,** 3743–3750
43. Wang, P., Wu, F., Ma, Y., Li, L., Lai, R., and Young, L. C. (2010) Functional characterization of the kinase activation loop in nucleophosmin (NPM)-anaplastic lymphoma kinase (ALK) using tandem affinity purification and liquid chromatography-mass spectrometry. *J. Biol. Chem.* **285,** 95–103
44. Morgan, R., Smith, S. D., Hecht, B. K., Christy, V., Mellentin, J. D., Warnke, R., and Cleary, M. L. (1989) Lack of involvement of the c-fms and N-myc genes by chromosomal translocation t(2;5)(p23;q35) common to malignancies with features of so-called malignant histiocytosis. *Blood* **73,** 2155–2164
45. Wang, N., Xie, C., Young, J. B., and Li, L. (2009) Off-line two-dimensional liquid chromatography with maximized sample loading to reversed-phase liquid chromatography-electrospray ionization tandem mass spectrometry for shotgun proteome analysis. *Anal. Chem.* **81,** 1049–1060
46. Wang, N., and Li, L. (2008) Exploring the precursor ion exclusion feature of liquid chromatography-electrospray ionization quadrupole time-of-flight mass spectrometry for improving protein identification in shotgun proteome analysis. *Anal. Chem.* **80,** 4696–4710
47. Elias, J. E., and Gygi, S. P. (2007) Target-decoy search strategy for increased confidence in large-scale protein identifications by mass spectrometry. *Nat. Methods* **4,** 207–214
48. Ghobrial, I. M., McCormick, D. J., Kaufmann, S. H., Leontovich, A. A., Loegering, D. A., Dai, N. T., Krajnik, K. L., Stenson, M. J., Melhem, M. F., Novak, A. J., Ansell, S. M., and Witzig, T. E. (2005) Proteomic analysis of mantle-cell lymphoma by protein microarray. *Blood* **105,** 3722–3730
49. Smith, L., Watson, M. B., O'Kane, S. L., Drew, P. J., Lind, M. J., and Cawkwell, L. (2006) The analysis of doxorubicin resistance in human breast cancer cells using antibody microarrays. *Mol. Cancer Ther.* **5,** 2115–2120
50. Shi, X., Franko, B., Frantz, C., Amin, H. M., and Lai, R. (2006) JSI-124 (cucurbitacin I) inhibits Janus kinase-3/signal transducer and activator of transcription-3 signalling, downregulates nucleophosmin-anaplastic lymphoma kinase (ALK), and induces apoptosis in ALK-positive anaplastic large cell lymphoma cells. *Br. J. Haematol.* **135,** 26–32
51. Amin, H. M., Medeiros, L. J., Ma, Y., Feretzaki, M., Das, P., Leventaki, V., Rassidakis, G. Z., O'Connor, S. L., McDonnell, T. J., and Lai, R. (2003) Inhibition of JAK3 induces apoptosis and decreases anaplastic lymphoma kinase activity in anaplastic large cell lymphoma. *Oncogene* **22,** 5399–5407
52. Bard, J. D., Gelebart, P., Anand, M., Amin, H. M., and Lai, R. (2008) Aberrant expression of IL-22 receptor 1 and autocrine IL-22 stimulation contribute to tumorigenicity in ALK+ anaplastic large cell lymphoma. *Leukemia* **22,** 1595–1603
53. Zhang, Z., and Zhang, R. (2008) Proteasome activator PA28 gamma regulates p53 by enhancing its MDM2-mediated degradation. *EMBO J.* **27,** 852–864
54. Feng, X., Guo, Z., Nourbakhsh, M., Hauser, H., Ganster, R., Shao, L., and Geller, D. A. (2002) Identification of a negative response element in the human inducible nitric-oxide synthase (hiNOS) promoter: The role of NF-kappa B-repressing factor (NRF) in basal repression of the hiNOS gene. *Proc. Natl. Acad. Sci. U.S.A.* **99,** 14212–14217
55. Xie, X., Wang, Z., and Chen, Y. (2007) Association of LKB1 with a WD-repeat protein WDR6 is implicated in cell growth arrest and p27(Kip1) induction. *Mol. Cell. Biochem.* **301,** 115–122
56. Kimura, S. H., Tsuruga, H., Yabuta, N., Endo, Y., and Nojima, H. (1997) Structure, expression, and chromosomal localization of human GAK. *Genomics* **44,** 179–187
57. Greener, T., Zhao, X., Nojima, H., Eisenberg, E., and Greene, L. E. (2000) Role of cyclin G-associated kinase in uncoating clathrin-coated vesicles from non-neuronal cells. *J. Biol. Chem.* **275,** 1365–1370
58. Byrd, D. A., Sweet, D. J., Panté, N., Konstantinov, K. N., Guan, T., Saphire, A. C., Mitchell, P. J., Cooper, C. S., Aebi, U., and Gerace, L. (1994) Tpr, a large coiled coil protein whose amino terminus is involved in activation of oncogenic kinases, is localized to the cytoplasmic surface of the nuclear pore complex. *J. Cell Biol.* **127,** 1515–1526
59. Nühse, T. S., Stensballe, A., Jensen, O. N., and Peck, S. C. (2003) Large-scale analysis of in vivo phosphorylated membrane proteins by immobilized metal ion affinity chromatography and mass spectrometry. *Mol. Cell. Proteomics* **2,** 1234–1243
60. Tsai, C. F., Wang, Y. T., Chen, Y. R., Lai, C. Y., Lin, P. Y., Pan, K. T., Chen, J. Y., Khoo, K. H., and Chen, Y. J. (2008) Immobilized metal affinity chromatography revisited: pH/acid control toward high selectivity in phosphoproteomics. *J. Proteome Res.* **7,** 4058–4069
61. Kokubu, M., Ishihama, Y., Sato, T., Nagasu, T., and Oda, Y. (2005) Specificity of immobilized metal affinity-based IMAC/C18 tip enrichment of phosphopeptides for protein phosphorylation analysis. *Anal. Chem.* **77,** 5144–5154
62. Wang, P., Zhang, J., Bellail, A., Jiang, W., Hugh, J., Kneteman, N. M., and Hao, C. (2007) Inhibition of RIP and c-FLIP enhances TRAIL-induced apoptosis in pancreatic cancer cells. *Cell. Signal.* **19,** 2237–2246
63. Wang, P., Song, J. H., Song, D. K., Zhang, J., and Hao, C. (2006) Role of death receptor and mitochondrial pathways in conventional chemotherapy drug induction of apoptosis. *Cell. Signal.* **18,** 1528–1535
64. Sethi, G., Sung, B., and Aggarwal, B. B. (2008) TNF: a master switch for inflammation to cancer. *Front. Biosci.* **13,** 5094–5107
65. Williams, G. M. (2008) Antitumor necrosis factor-alpha therapy and potential cancer inhibition. *Eur. J. Cancer Prev.* **17,** 169–177
66. Devin, A., Lin, Y., and Liu, Z. G. (2003) The role of the death-domain kinase RIP in tumour-necrosis-factor-induced activation of mitogen-activated protein kinases. *EMBO Rep.* **4,** 623–627
67. Meylan, E., and Tschopp, J. (2005) The RIP kinases: crucial integrators of cellular stress. *Trends Biochem. Sci.* **30,** 151–159
68. Song, H. Y., Dunbar, J. D., Zhang, Y. X., Guo, D., and Donner, D. B. (1995) Identification of a protein with homology to hsp90 that binds the type 1 tumor necrosis factor receptor. *J. Biol. Chem.* **270,** 3574–3581
69. Pridgeon, J. W., Olzmann, J. A., Chin, L. S., and Li, L. (2007) PINK1 protects against oxidative stress by phosphorylating mitochondrial chaperone TRAP1. *PLoS Biol.* **5,** e172
70. Brill, L. M., Salomon, A. R., Ficarro, S. B., Mukherji, M., Stettler-Gill, M., and Peters, E. C. (2004) Robust phosphoproteomic profiling of tyrosine phosphorylation sites from human T cells using immobilized metal affinity chromatography and tandem mass spectrometry. *Anal. Chem.* **76,** 2763–2772
71. Zhang, Q., Raghunath, P. N., Xue, L., Majewski, M., Carpentieri, D. F., Odum, N., Morris, S., Skorski, T., and Wasik, M. A. (2002) Multilevel dysregulation of STAT3 activation in anaplastic lymphoma kinase-positive T/null-cell lymphoma. *J. Immunol.* **168,** 466–474
72. Fujimoto, J., Shiota, M., Iwahara, T., Seki, N., Satoh, H., Mori, S., and Yamamoto, T. (1996) Characterization of the transforming activity of p80, a hyperphosphorylated protein in a Ki-1 lymphoma cell line with chromosomal translocation t(2;5). *Proc. Natl. Acad. Sci. U.S.A.* **93,** 4181–4186
73. Voena, C., Conte, C., Ambrogio, C., Boeri Erba, E., Boccalatte, F., Moham-

med, S., Jensen, O. N., Palestro, G., Inghirami, G., and Chiarle, R. (2007) The tyrosine phosphatase Shp2 interacts with NPM-ALK and regulates anaplastic lymphoma cell growth and migration. *Cancer Res.* **67,** 4278–4286

74. Ruchatz, H., Coluccia, A. M., Stano, P., Marchesi, E., and Gambacorti-Passerini, C. (2003) Constitutive activation of Jak2 contributes to proliferation and resistance to apoptosis in NPM/ALK-transformed cells. *Exp. Hematol.* **31,** 309–315
75. Nieborowska-Skorska, M., Slupianek, A., Xue, L., Zhang, Q., Raghunath, P. N., Hoser, G., Wasik, M. A., Morris, S. W., and Skorski, T. (2001) Role of signal transducer and activator of transcription 5 in nucleophosmin/anaplastic lymphoma kinase-mediated malignant transformation of lymphoid cells. *Cancer Res.* **61,** 6517–6523
76. Fawal, M., Armstrong, F., Ollier, S., Dupont, H., Touriol, C., Monsarrat, B., Delsol, G., Payrastre, B., and Morello, D. (2006) A "liaison dangereuse" between AUF1/hnRNPD and the oncogenic tyrosine kinase NPM-ALK. *Blood* **108,** 2780–2788
77. Cussac, D., Greenland, C., Roche, S., Bai, R. Y., Duyster, J., Morris, S. W., Delsol, G., Allouche, M., and Payrastre, B. (2004) Nucleophosmin-anaplastic lymphoma kinase of anaplastic large-cell lymphoma recruits, activates, and uses pp60c-src to mediate its mitogenicity. *Blood* **103,** 1464–1471
78. Galietta, A., Gunby, R. H., Redaelli, S., Stano, P., Carniti, C., Bachi, A., Tucker, P. W., Tartari, C. J., Huang, C. J., Colombo, E., Pulford, K., Puttini, M., Piazza, R. G., Ruchatz, H., Villa, A., Donella-Deana, A., Marin, O., Perrotti, D., and Gambacorti-Passerini, C. (2007) NPM/ALK binds and phosphorylates the RNA/DNA-binding protein PSF in anaplastic large-cell lymphoma. *Blood* **110,** 2600–2609
79. Colomba, A., Courilleau, D., Ramel, D., Billadeau, D. D., Espinos, E., Delsol, G., Payrastre, B., and Gaits-Iacovoni, F. (2008) Activation of Rac1 and the exchange factor Vav3 are involved in NPM-ALK signaling in anaplastic large cell lymphomas. *Oncogene* **27,** 2728–2736
80. Shi, P., Lai, R., Lin, Q., Iqbal, A. S., Young, L. C., Kwak, L. W., Ford, R. J., and Amin, H. M. (2009) IGF-IR tyrosine kinase interacts with NPM-ALK oncogene to induce survival of T-cell ALK+ anaplastic large-cell lymphoma cells. *Blood* **114,** 360–370